# Final Report of the K-112964
# „Vascular effects of sphingolipid mediators”
# Research Project

## I. Role of S1P in the regulation of vascular tone and reactivity

Our first aim was to characterize the vasoactive effects of sphingosine-1-phosphate (S1P) in our experimental model. In phenylephrine (PE) precontracted mouse aortic segments, S1P typically evoked a tri-phasic response consisting of a transient constriction followed by a marked relaxation and finally a tonic constriction. In order to dissect the relaxant and constrictor components of the response, the effects of S1P in vessels of endothelial nitric oxide synthase knockout (eNOS KO) animals were tested, as endothelial NO has been reported to mediate S1P-induced vasorelaxation. Indeed, in the absence of eNOS S1P evoked strong and sustained vasoconstriction.

In order to gain in depth insight into this vasoconstrictor effect, the experiments were repeated with administration of S1P on the resting tone (RT) of the vessels. Our results showed that S1P induced only minor vasoconstriction in both wild-type (WT) and eNOS KO vessels. Based on these results we concluded that S1P is a weak vasoconstrictor by itself, however, it can significantly enhance the contractile effect of α1 adrenoreceptor stimulation.

To test this hypothesis, the following experimental protocol was used. PE was administered at increasing concentrations (0.1 nM–10 μM) enabling the evaluation of the dose-response-relationship. Between two PE administrations, S1P (5 μM) was applied for 20 min followed by washing. PE-induced vasoconstriction of the vessels increased markedly after exposure to S1P: the Emax value increased whereas the EC50 decreased significantly, whereas the vehicle of S1P had no effect.

Our next aim was to identify the receptor subtype mediating S1P-induced potentiation of α1-adrenergic vasoconstriction. First, a smooth muscle specific S1P1 receptor deficient mouse line (SM-S1P1-KO) was generated by crossing S1P1-floxed mice with the smooth muscle specific SMMHC-Cre line as general S1P deficiency results in embryonic lethality. However, in vessels of SM-S1P1-KO mice the effect of S1P on the α1-adrenergic vascular reactivity remained unaltered. Thereafter, we tested vessels isolated from S1P2 KO and S1P3 KO animals and their corresponding controls. In control vessels the marked potentiation of PE-induced vasoconstriction was present after incubation with S1P. In contrast, the potentiating effect of S1P failed to develop in S1P2 KO vessels, whereas it remained unaltered in S1P3 KO vessels. These observations unambiguously indicated the exclusive role of S1P2 in mediating the enhanced vascular response to PE after exposure to S1P.

The next step was to identify the intracellular signaling pathway by testing vessels deficient for $G\alpha_{12}$ and $G\alpha_{13}$ proteins in smooth muscle cells. Whereas control vessels showed the potentiating effect of S1P on α1-adrenergic vasoconstriction, this effect was abolished in $G\alpha_{12/13}$ KO mice, indicating the role of $G_{12/13}$ signaling in S1P-induced potentiating effect. As $G\alpha_{12/13}$ proteins can activate reportedly the RhoA - Rho kinase (ROCK) signaling pathway, we evaluated its involvement in mediating the effect of S1P on vascular reactivity. In accordance to our hypothesis, the ROCK inhibitors Y-27632 and fasudil were able to prevent the development of S1P-induced potentiation of α1-adrenergic vasoconstriction.

We also aimed to investigate the duration of the potentiating effect of S1P. Identical doses of PE were applied at 20-minute intervals, and the magnitude of contraction responses was measured. Enhanced PE-induced contractions were detected for three hours after exposure to S1P in WT vessels. This long-lasting vascular hyper-reactivity failed to develop in S1P2 KO but remained unaltered in S1P3 KO vessels.

In conclusion, S1P induced vascular hyper-reactivity to α1-adrenergic stimulation of vascular smooth muscle cells. We confirmed that the signaling pathway involves S1P2 receptor, $G\alpha_{12/13}$ proteins and ROCK. This is supported by the observations that the potentiating effect of S1P was absent in of S1P2 KO or $G\alpha_{12/13}$ KO vessels and could be abolished by the ROCK inhibitor Y-27632 and fasudil.

The intracellular signaling pathways activated by S1P and α1-adrenergic receptors finally converge in the cross-bridge cycle where α1-adrenergic signaling drives myosin light chain kinase (MLCK)-mediated myosin phosphorylation, whereas S1P2 signaling induces retention of the phosphorylated state of myosin by inhibition of myosin phosphatase (MP), maintaining the cross-bridge cycle active and allowing for the development of sustained vasoconstriction. In order to verify this concept, we planned additional experiments in which the MLCK activation is achieved by a GPCR-independent mechanism, such as potassium-induced membrane depolarization and consequent opening of voltage-gated $Ca^{2+}$ channels.

Aortic segments were isolated from WT, as well as S1P2, S1P3 receptor, and $G\alpha_{12/13}$ KO mice and their isometric tension was measured in myographs after removal of the endothelium. Vasoactive effect of 10 μM S1P was detected at physiological (4 mM) as well as at elevated (6-8 mM) extracellular potassium concentrations ($[K^+]_e$). At physiological $[K^+]_e$ S1P slightly increased the vascular tone, whereas sphingosine had no measurable effect. Moderately increased $[K^+]_e$ (6 mM) failed to influence the vascular tone by itself, but addition of S1P induced marked vasoconstriction that was further increased when $[K^+]_e$ was elevated to 8 mM.

Further experiments on the signaling of vascular smooth muscle contraction were performed with 8 mM $[K^+]_e$, since it intensified the vasoactive action of S1P without having a significant influence on the resting vascular tone by itself. The vasoconstrictor effect of S1P was diminished in S1P2 KO and $G\alpha_{12/13}$ KO vessels, whereas it remained unchanged in vessels of S1P3 KO mice. S1P-induced vasoconstriction was also strongly decreased by the Rho-kinase inhibitor Y-27632 in WT vessels.

In conclusion, S1P significantly elevates the VSM tone in isolated mouse aorta under moderately increased K+-concentration. This effect is mediated by the S1P2-receptor, $G\alpha_{12/13}$ proteins, and the activation of Rho-kinase. This phenomenon may contribute to the pathological increase of the vascular tone under conditions of systemic hyperkalemia, like in kidney diseases, or during local elevation of perivascular $[K^+]_e$ in hypoxic tissues, eg. during myocardial ischemia.

## II. Effects of S1P and LPA on the coronary circulation

In this part of our study we made attempts to investigate the effects of S1P and the related lysophospholipid mediator lysophosphatidic acid (LPA) on the regulation of the coronary circulation and cardiac functions. We also investigated the potential receptors and intracellular pathways that may mediate those effects. Potential cardioprotective effect of S1P has also been studied, because S1P is released reportedly in large amounts in acute coronary syndrome (ACS), and may evoke both favorable and potentially deleterious effects. We aimed to delineate how these conflicting S1P actions indeed affect postischemic cardiac injury.

LPA is known to act on 6 documented G protein-coupled receptors (LPA1-6), of which LPA1-3, together with S1P1-5, belong to the endothelial differentiation gene (Edg) family of G-protein coupled receptors (GPCRs). Similarly to S1P, LPA has diverse effects in the cardiovascular system including regulation of the vascular tone. Although several LPA species are released in ACS, the effects of LPA on coronary vascular tone remain to be elucidated. Our aim was to describe the effects of S1P and LPA on the coronary flow of isolated murine hearts and to identify the signaling pathways mediating the effect.

Experiments were conducted on isolated Langendorff-perfused hearts of 130-150-days-old male mice. Coronary flow was continuously monitored with a transit-time flow meter placed into the inflow line. In order to measure left ventricular pressure a fluid filled balloon-catheter connected to a pressure transducer was inserted into the ventricle. After cannulation, a 30-minute-long stabilization period was allowed. After equilibration, control data were recorded and S1P, LPA or their vehicle was infused to the perfusion line for 5 minutes. Afterwards, depending on the protocol either a 20-minute-long washout period or a 30-minute-long global ischemia was applied by complete cessation of perfusion. At the end of the ischemic period, perfusion was reintroduced and reperfusion was followed up for 2 hours. Size of the infarcted myocardium was determined through TTC staining. Experiments were carried out in WT and various gene-deficient C57/Bl6 mice strains.

To investigate the effects of S1P on CF and cardiac function we infused $10^{-6}$ M S1P or its vehicle to the perfusate of isolated WT murine hearts for 5 min. Administration of S1P reduced CF by 44%. This remarkable decrease started at the beginning of the S1P infusion and continued progressively during the 5 minutes. During the wash-out period CF did not return to the control state but remained at a significantly lower level

CF reduction induced by S1P compromised left ventricular contractile performance which is evidenced by a 54% drop of left ventricular developed pressure (LVDevP) and decreased $+dLVP/dt_{max}$ and $-dLVP/dt_{max}$ (indices of inotropic and lusitropic functions, respectively), indicating insufficient oxygen supply to the myocardium.

Earlier studies suggested that S1P may affect coronaries via S1P1, S1P2 and S1P3 receptors. Therefore, as a next step we aimed to identify which of these receptors mediate the coronary actions of S1P observed in our experiments. For this purpose, we perfused S1P to isolated hearts of smooth muscle specific conductional S1P1, as well as conventional S1P2 and S1P3 gene deficient mice following the protocol described above.

The CF reducing effect of S1P in S1P1 and S1P2 deficient hearts was similar to that observed in WTs. The drop of the LVDevP was also similar, no statistically significant difference could be detected.

In S1P3 KO hearts, however, the CF reducing effect of S1P was significantly diminished compared to WT mice: both the maximal effects the total perfusion deficit during the 5-minute-long S1P infusion decreased by approximately 50%. The decrease in left ventricular contractile performance upon S1P infusion was also attenuated in S1P3 KO mice: the drop in LVDevP was significantly smaller compared to controls.

In mouse experimental models used for the identification of intracellular signaling pathways, the smooth muscle specific deletion of $G\alpha_{q/11}$ or $G\alpha_{12/13}$ did not influence the effect of S1P on the coronary flow. Moreover, inhibition of endothelin A receptor by BQ123 ($10^{-6}$ M) could not abolish its effect either.

To solve the contradiction between the well-known cardioprotective and observed cardiac function reducing effect of S1P we aimed to separate the role „vascular" and „myocardial" effects of S1P.

First, we investigated the role of the "vascular" S1P. S1P pretreatment was carried out by infusing S1P to the perfusion solution before ischemia. During the reperfusion period CF returned to a significantly higher value in the S1P3 KO hearts. Surprisingly, however, the recovery of the cardiac function and infarct size did not differ remarkably in the two groups.

Second, we investigated the role of „myocardial" S1P released endogenously from the heart. In this protocol, no S1P has been applied to the perfusion line. Interestingly, under these conditions CF during the reperfusion period did not differ significantly between WT and S1P3 KO hearts. On the contrary, parameters representing cardiac function did remarkably show difference. Loss of the S1P3 receptor resulted in a far worse recovery of the cardiac function. In addition, the infarct size was also larger in S1P3 KO than in WT hearts.

In conclusion, S1P is a strong vasoconstrictor in the coronaries. After the exclusion of the S1P1 and S1P2 our results indicate that the coronary constrictor effect of S1P is mediated, at least in part, via the S1P3 receptor. The $G\alpha_{q/11}$ and the $G\alpha_{12/13}$ proteins

and the endothelin A receptor are not involved in mediating the CF reducing effect of S1P. In contrast, myocardium-derived S1P appears to improve cardiac functions during ischemia/reperfusion, an effect mediated probably by myocardial S1P3 receptors.

In a separate set of experiments, we aimed to investigate the effects of LPA on the coronary circulation and the signaling mechanism involved. Because unsaturated LPA species are also released reportedly in acute coronary syndrome, effects of various LPA species (18:1, 18:2 and 18:3 LPA) were determined on the CF of isolated murine hearts.

To investigate the effects of LPA on CF and cardiac function we infused $10^{-6}$ M LPA or its vehicle to the perfusate of isolated WT murine hearts for 5 min. Administration of LPA reduced CF by 37%. This remarkable decrease started at the beginning of LPA infusion and remained stable during the 5 minutes. During the wash-out period CF returned to the control state. CF reduction induced by LPA compromised left ventricular contractile performance which is evidenced by the drop of LVDevP and decreased $+dLVP/dt_{max}$ and $-dLVP/dt_{max}$.

Next, we aimed to identify the LPA receptor mediating the CF reducing effect of LPA. Expression analysis by qPCR indicated the presence of all 6 known LPA receptors in the heart. CF reducing effect of LPA developing in LPA1 and LPA2 deficient mice was similar to that of WT littermates. The drop of the LVDevP was also similar, no statistically significant difference could be detected. In the presence of LPA3 antagonists (Ki16425 and VPC32183) similar results were detected.

Then we started to investigate the members of the non-Edg LPA receptors (LPA4-6). Both in LPA4 KO hearts and in the presence of the LPA4 antagonist BrP-LPA the CF reducing effect of LPA was significantly diminished compared to WT mice. The decrease in left ventricular contractile performance upon LPA infusion was also attenuated: the drop in LVDevP was significantly smaller compared to controls.

In mouse experimental models used for the identification of intracellular signaling pathways, the smooth muscle specific deletion of $G\alpha_{q/11}$ did not influence the effect of LPA on the coronary flow whereas that of $G\alpha_{12/13}$ diminished by 50% the CF reduction. The ROCK inhibitor Y27632 abolished the effect of LPA on CF. Moreover, deletion of endothelial NO synthase enhanced, whereas inhibition of endothelin A receptor by BQ123 diminished the response of coronaries to LPA.

Taken together, unsaturated 18C LPA species are strong vasoconstrictors in the coronaries. LPA4 receptors, endothelin-1 and the $G_{12/13}$ - ROCK signaling pathway are involved in mediating the coronary vasoconstriction.

These vascular changes might have pathophysiological importance in platelet activation and sclerotic plaque rupture when large amount of S1P and LPA are released in the coronary system.

## 3. Effects of sphingolipids on endothelium-dependent, NO-mediated vasodilatation

Sphingolipid mediators may induce biological actions independently of S1P receptors. In many cases a direct interaction of sphingolipids with intracellular signaling molecules is responsible for mediating these effects. Károly Liliom and his co-workers have recently demonstrated a molecular interaction between sphingolipids (sphingosine and dimethylsphingosine (DMS)) and the calcium-binding protein calmodulin, resulting in an inhibition of the activity of the $Ca^{2+}$/calmodulin regulated eNOS enzyme. We hypothesized that this interaction may have consequences on the endothelium-dependent vascular reactivity. In order to test this hypothesis, we determined the effect of sphingosine and DMS (10 and 50 μM) on the eNOS-mediated vasodilator effect of acetylcholine (ACh).

Sphingosine and DMS induced significant reduction of ACh-induced vasodilation whereas the effects of the NO-donor sodium nitroprusside (SNP) remained unaltered, indicating that the endothelial release but not the smooth muscle action of NO was altered in the presence of sphingolipids. With these results we proved that the interaction of sphingosine and DMS with the $Ca^{2+}$/calmodulin – eNOS pathway is relevant in the regulation of the vascular tone. In further experiments we aimed to test whether sphingosine may alter the blood pressure via its effect on the vascular reactivity. Sphingosine applied in doses up to 3 nmol/g intravenously or 30 nmol/g intraperitoneally failed to induce significant changes of the blood pressure. Unfortunately, however, in these experiments the distribution of the systemically applied sphingosine in the body was obscure, and several processes (eg. glomerular filtration, binding to plasma or cell surface proteins, uptake and/or metabolism by non-endothelial cells) could hinder the endothelial actions of sphingosine. Nevertheless, we can conclude that local rather than systemic release of sphingolipids may have an impact in the regulation or dysregulation of vascular tone,

MLCK in the smooth muscle, another key regulator of the vascular tone, is also a $Ca^{2+}$/calmodulin regulated enzyme. In order to test the inhibitory effect of sphingosine and DMS on MLCK activity in the smooth muscle, we tested whether these sphingolipids are able to inhibit the contractile effect of phenylephrine (PE). Surprisingly, we found that Sph and DMS increase PE-induced vasoconstriction. As the aforementioned inhibition of NO production can indirectly lead to augmented vasoconstrictor responses, we repeated the experiments on vessels prepared from eNOS KO animals. Sph and DMS were unable to increase PE-induced vasoconstriction in these vessels, indicating that the sphingolipid-induced enhancement of vascular reactivity is probably mediated by inhibition of eNOS.

With these results we proved that the interaction of sphingosine/DMS with the $Ca^{2+}$/calmodulin – eNOS pathway is relevant in the regulation of the vascular tone. However, Sph and DMS do not have any significant direct effect on MLCK activity in the vascular smooth muscle.

## 4. Vasoactive actions of sphingomyelinase in type 2 diabetes

Sphingomyelinase (SMase) catalyzes the conversion of the phospholipid sphingomyelin to ceramide, which is the precursor of other sphingolipid mediators, like sphingosine and S1P. SMase enzymes are reportedly upregulated in certain cardiovascular and metabolic disorders such as type 2 diabetes mellitus (T2DM). Sphingolipids have also been implicated as important regulators of inflammatory processes in diabetes. Stress conditions initiate changes in sphingolipid metabolism, and sphingolipids have emerged as key mediators of stress responses. In spite of the marked alterations in the metabolism and actions of sphingolipids in diabetes and recent observations indicating that ceramide may contribute to the development of diabetic endothelial dysfunction, relatively little is known about the effects of sphingolipids on vascular functions in T2DM.

We aimed to analyze the effects of SMase on vascular tone under diabetic conditions and to elucidate the signal transduction mechanisms involved. Application of 0.2 U/ml nSMase evoked a complex vascular effect with dominant contraction in control vessels and a more pronounced relaxation in vessels of db/db mice, a rodent model of T2DM. After inhibition of the TP receptor by 1 μM SQ 29,548, 0.2 U/ml nSMase relaxed both db/db and control vessels, with a significantly higher relaxation in the db/db group. After incubation of the vessels with 1 μM SQ 29,548 and 100 μM L-NAME for 30 minutes, 0.2 U/ml nSMase could no longer evoke a tension change in the thoracic aorta of control or db/db mice.

Taken together, in our experiments we have observed an unexpected enhancement of SMase-induced, NO-mediated vasorelaxations in type 2 diabetic db/db mice, in contrast to the diminished vasorelaxant effect of ACh.

In order to understand the mechanism of SMase induced vasorelaxation, the effects of inhibitors of certain intracellular signaling pathways have been determined. The S1P1 receptor antagonist W146 (1 μM), the ceramidase inhibitor D-erythro-MAPP (50 μM), the PI3-kinase inhibitor Wortmannin (100 nM) and the protein kinase B/Akt inhibitor MK 2206 (1 μM) all failed to alter the vasoactive effects of SMase both in WT control and in db/db mice. In contrast, propargylglycine (PAG, 10 mM) induced inhibition of cystathionine-γ-liase (CSE), the enzyme mediating endogenous hydrogen sulfide ($H_2S$) production, attenuated the vasodilator effect of SMase in vessels of db/db mice. In addition, enhanced vasorelaxant responses to exogenous $H_2S$ were observed in these vessels. These results indicate that the increased vasorelaxation induced by SMase in vessels of type 2 diabetic mice is related to elevated endogenous $H_2S$ production and/or the enhanced reactivity of the vascular smooth muscle to $H_2S$. Since $H_2S$ reportedly augments the vascular actions of NO by inhibiting the activity of the cGMP-specific phosphodiesterase-5, SMase may attenuate diabetes-induced vascular dysfunction by reversing the consequences of diminished NO bioavailability.

## 5. Signal transduction mechanism of lysophosphatidic acid induced vasoconstriction

According to our previous studies, LPA evokes vasoconstriction when the endothelium is damaged or the eNOS enzyme is knocked out. To understand the signal transduction mechanism of this vasoconstriction, we first evaluated the expression levels of all known LPA receptors in isolated aortic smooth muscle cells. LPA1, LPA2, LPA4 and LPA6 transcripts were abundantly detectable by qPCR both in thoracic and abdominal aortae.

Further experiments were carried out on endothelium denuded abdominal aorta segments, isometric tension was recorded with wire myograph. Oleoyl-LPA and the LPA1-3 receptor agonist VPC31143 both evoked vasoconstriction. Since the synthetic agonist showed a higher efficacy over the natural ligand in inducing constriction, we used the VPC31143 for further investigations.

Ki16425, an antagonist of LPA1 and LPA3 receptors blocked the effect of VPC31143, while DGPP, a selective antagonist of only the LPA3 receptor was ineffective. Vessels prepared from LPA2 KO animals showed unchanged constriction to VPC31143, however the constriction was diminished in LPA1 knockouts. We also checked the effect of T13, which according to literal data is a selective LPA3 agonist in low nanomolar (10 nM) concentration but can activate other LPA receptors at higher concentrations. T13 failed to induce contraction when 10 nM was applied but higher concentrations evoked a dose-dependent vasoconstriction. As this constriction was missing in LPA1 knockouts, we concluded that LPA1 receptors are the exclusive mediators of the vasoconstriction.

Because it is known that LPA has COX1-dependent effects and indomethacin blocks the constrictor effect of LPA in the small intestine, we hypothesized that $TXA_2$ might mediate the constrictor effect of LPA. To test this, we repeated the myograph measurements in COX1 KO and TP KO vessels and have found a reduced vasoconstriction in these specimens. Thromboxane production of the vessels was also tested by $TXB_2$ ELISA. In WT vessels, baseline thromboxane production increased two-three folds after VPC31143. A similar increase was detectable in LPA2 KO and TP KO vessels, while in LPA1 KO and COX1 KO vessels VPC31143 was not able to increase thromboxane production.

A known pathway for thromboxane production is the pertussis toxin (PTX)-sensitive $G_i$ and consequent $PLA_2$ activation. We have found that PTX treatment strongly decreases both VPC31143-mediated vasoconstriction and thromboxane production.

According to our findings LPA1 receptor activation in aortic smooth muscle evokes vasoconstriction via $G_{i/o}$- and COX1-mediated autocrine/paracrine thromboxane release and consequent TP receptor activation.

# Copies of yet unpublished manuscripts

1. Dina Wafa, Nóra Koch, Janka Kovács, Margit Kerék, Zoltán Benyó, Zsuzsanna Miklós: Dual effect of $S1P_3$ receptors on myocardial functions.

2. Tünde Juhász, Éva Ruisanchez, Veronika Harmat, József Kardos, Mónika Kabai, Viktor Erdősi, Zoltán Benyó, Károly Liliom: Sphingosine inhibits calmodulin action: Implication for regulation of endothelial nitric oxide synthase-mediated vasorelaxation.

3. Éva Ruisanchez, Rita Cecília Panta, Levente Kiss, Zsuzsa Straky, Dávid Korda, Adrienn Párkányi, Károly Liliom, Gábor Tigyi, Zoltán Benyó: Enhanced endothelial nitric oxide mediated vasorelaxation by sphingomyelinase in db/db mice.

cells

MDPI

*Article*

# Dual effect of $S1P_3$ receptors on myocardial functions

**Dina Wafa[1], Nóra Koch [1], Janka Kovács [1], Margit Kerék [1], Zoltán Benyó [1], Zsuzsanna Miklós [1]**

[1]Semmelweis University, Institute of Translational Medicine, 1094 Budapest, Hungary; dina.wafa.93@gmail.com, kochnori@gmail.com, kovacsjankee@gmail.com, margit.nagy9@gmail.com, benyo.zoltan@med.semmelweis-univ.hu, miklos.zsuzsanna@med.semmelweis-univ.hu

Received: date; Accepted: date; Published: date

**Abstract:** Sphingosine-1-phosphate (S1P) is a lysophospholipid mediator which regulates diverse biological processes through its specific receptors ($S1P_{1-5}$). S1P has been shown to be protective against ischemia/reperfusion (I/R) injury in the heart. Other studies highlighted its constrictive effects in the coronaries. S1P is released from platelets in acute coronary syndrome (ACS) in large amounts therefore its favorable and potentially deleterious effects may be conflicted. Experiments were conducted on isolated Langendorff-perfused hearts. S1P infusion or I/R protocol was applied on WT, $S1P_2$ and $S1P_3$ gene-deficient mice. Coronary flow (CF), contractile function and infarct size was determined. Administration of S1P reduced CF by 48±8% and compromised left ventricular contractile performance in WT hearts. These effects in $S1P_2$ KO mice were similar. In $S1P_3$ KO hearts the CF reduction (25±2%) and decline in contractile function were diminished. In I/R experiments, postischemic functional recovery was weaker and infarct size was larger in $S1P_3$ KO hearts. Preischemic S1P treatment worsened the recovery of CF and contractile function both in WT and $S1P_3$ KO hearts. S1P reduced CF and contractile function massively mediated via $S1P_3$ receptor. We verified the role of $S1P_3$ receptor in cardioprotection, but not the S1P pretreatment that just further exacerbated I/R-induced myocardial damage.

**Keywords:** sphingosine-1-phosphate, ischemia/reperfusion, cardioprotection, vasoconstriction, coronary flow, contractile function, infarct size

## Introduction

Ischaemic heart disease, including acute coronary syndrome (ACS), is the major cause of death globally. ACS is the sudden loss of adequate blood perfusion to the heart, most commonly initiated by the rupture of an atherosclerotic plaque and consequential activation of blood coagulation. This process ends up in thrombotic occlusion of the coronary and cardiac tissue damage (1). Urgent reestablishment of blood perfusion to the affected area is crucial to minimize ischemic tissue damage. Besides the therapeutic window the success of reperfusion depends on several other factors such as pathophysiological events happening prior to and during thrombus formation. Platelet activation can be relevant in this respect, as it releases numerous vasoactive mediators which may have impact on the dynamics and severity of ischemic injury. Sphingosine-1-posphate (S1P) is one of these many mediators.

S1P is a sphingolipid mediator which is produced by a wide variety of cells. Its actions include regulation of diverse physiological and pathophysiological processes, such as inflammation, autoimmunity and neurodegeneration (2)(3). In the cardiovascular (CV) system activated platelets synthetize and release it in large amounts (4) and it has been reported to play a role in the regulation of vascular tone, atherogenesis, cardiac remodeling and cardioprotection (5)(6)(7). To date, 5 different G-protein coupled receptors belonging to the Edg family have been identified as specific S1P receptors ($S1P_{1-5}$). From these, $S1P_1$, $S1P_2$ and $S1P_3$ receptors

are expressed abundantly in the CV system and has been reported to mediate CV actions of S1P (8)(9).

S1P has been attributed cardioprotective effects against ischemia-reperfusion (I/R) injury by several research groups. The key enzymes in S1P synthesis, sphyngosine-kinase 1 and 2 (SphK1 and 2) were associated with beneficial effects of ischemic pre-and post-conditioning and increased release of S1P from cardiomyocytes (10)(11)(12). Combined deletion of $S1P_2$ and $S1P_3$ receptors increased the infarcted area and enhanced apoptotic cell death after I/R, suggesting that activation of these receptors is cardioprotective. (13)

Preischemic S1P treatment has been reported to decrease infarct size in ex vivo experimental models (12). In vivo most of the S1P in the plasma is connected with HDL. It has been reported that HDL and S1P directly protect the heart against I/R injury via the $S1P_3$ receptor in vivo (14).

However in ACS when S1P is released in large amounts HDL is not bound to S1P. Along with that, some studies highlighted the potential constrictive effects of S1P in the coronaries. S1P administration to the coronary perfusate has been shown to diminish coronary flow (CF) in Langendorff-perfused rat hearts (15). This effect was attenuated by pharmacological inhibition of $S1P_3$ receptors in the same experiment (15). Another study conducted on coronary smooth muscle cells raised the potential involvement of $S1P_2$ receptors (16). Beside its actions on coronary flow, S1P exerts other short-term cardiac effects which include generation of arrhythmias and negative inotropy (17)(18)(19)(20).

The reported cardiac effects of S1P are contradictory with respect to I/R injury. Activation of S1P receptors seems to be cardioprotective on one hand, whereas acute effects of S1P to reduce CF and cardiac contractility are expected to interfere with successful post-ischemic recovery on the other. Moreover, $S1P_2$ and $S1P_3$ receptors have been shown to participate in each mechanism. In ACS, when S1P is released in large amounts from activated platelets, its favorable and potentially deleterious effects may be conflicted. In the present study, we aimed to delineate how these conflicting S1P actions actually affect postischemic cardiac injury after a non-fatal ischemic insult.

For this purpose, we conducted ex vivo experiments on isolated Langendorff-perfused murine hearts. In our experimental models firstly we mimicked ACS as a massive S1P release to the coronary system. Through gene-deficient mice we tried to characterize its meschanism of action. To understand the role of $S1P_3$ receptor in cardioprotection we applied an I/R protocol. Finally, to model S1P pretreatment, S1P was administered before I/R to investigate how its acute effects will influence S1P receptor mediated cardioprotection and postischemic cardiac recovery.

## Materials and Methods

### Animals

All experiments reported here were performed using 130-150-days-old male mice. Animals were housed in the animal facility at Semmelweis University, were kept in 12 hours' day and night condition and had free access to water and food. C57/Bl6 (WT) mice were originated from Charles River Laboratories (Isaszeg, Hungary). To answer our specific questions, we used conventional S1P2 KO and S1P3 KO animals along with wild-type littermates (S1pr2 (-/-) and S1pr3 (-/-) strains generated on C57/Bl6 genetic background, both were generous gift from

Richard L. Proia (NIDDK, NIH, MD, USA)). All procedures were approved by the National Food Chain Safety Office, Hungary (Permission number: PEI/001/820-2/2015).

**Isolated perfused heart experiments**

General anesthesia was induced by intraperitoneal injection of 40 mg/kg pentobarbital, followed by thoracotomy and isolation of the heart. After excision, the isolated heart was mounted in a Langendorff setup (Experimetria ltd., Budapest) and perfused at constant 80 mmHg pressure with modified Krebs-Henseleit buffer (118 mM NaCl, 4.3 mM KCl, 25 mM $NaHCO_3$, 1.2 mM $MgSO_4$, 1.2 mM $KH_2PO_4$, 0.5 mM NaEDTA, 2.0 mM $CaCl_2$, 11 mM glucose, 5 mM pyruvate- all purchased from Sigma-Aldrich, Budapest, Hungary). (21) The solution was continuously gassed with 95% $O_2$ and 5% $CO_2$ and had a pH of 7.4 at 37°C. During the experiment the heart was surrounded by a thermally regulated chamber filled with Krebs-Henseleit buffer.

Coronary flow was continuously monitored with a transit-time flow meter placed into the inflow line (Transonic 2PXN flow probe, Transonic Systems Inc., Ithaca, NY, USA). In order to measure left ventricular pressure (LVP) a fluid filled balloon-catheter connected to a pressure transducer was inserted into the ventricle. End diastolic pressure was set to 8 mmHg.

Devices were connected to a computer and data were recorded and analyzed by Haemosys (Experimetria, Budapest) software. Left ventricular developed pressure (LVDevP) was calculated as the difference of peak systolic and minimum diastolic pressures; and the positive and negative maximum values of the first derivative of the LVP ($+dLVP/dt_{max}$, $–dLVP/dt_{max}$) were determined as indices of left ventricular contractile and lusitropic performance, respectively.

*Experimental protocol*

After cannulation, a 30-minute-long stabilization period was allowed. After equilibration, control data were recorded and S1P (D-erythro-sphingosine-1-phosphate, Avanti Inc., $10^{-6}$ M) or vehiculum was infused to the perfusion line for 5 minutes. 1 mg S1P was dissolved in 263 microliter 0.3 N NaOH. This solution ($10^{-2}$ M) was further diluted to $10^{-4}$ M with saline and infused to the perfusate by $1/100^{th}$ of the CF to acquire a final concentration of $10^{-6}$ M in the coronaries. Afterwards, depending on the protocol either a 20-minute-long washout period or a 30-minute-long global ischemia was applied by complete cessation of perfusion. At the end of the ischemic period, perfusion was reintroduced and reperfusion was followed up for 2 hours.

**Measurement of infarct size**

In the ischemia/reperfusion experiments, hearts were removed from the cannula after the 2-hour-long reperfusion period and placed into a −20°C freezer for at least 15 minutes. The frozen heart was cut into 1 mm thick slices simply by eye. The slices were then incubated in a phosphate buffer containing 1% triphenyltetrazolium (TTC) (Sigma, Budapest, Hungary) for 15 minutes at a temperature of 37°C. The TTC powder was diluted in a two-part phosphate buffer system at a pH of 7.4. The surviving tissue turned deep red and the infarcted tissue remained pale. Slices were then fixed in 10% formalin for 20 minutes (22). Photos of the slices were captured using a strereomicroscope equipped with a high-resolution digital camera and Image J (Rasband, W.S., ImageJ, US National Institutes of Health, Bethesda, MD, USA, https://imagej.nih.gov/ij) was used to analyze them. The area at risk (total area, white plus red part) and the infarcted area (white part) were measured and the relative infarct size was calculated as a percentage of the area at risk.

### Statistical analysis

Results are presented as means ± standard error of the mean (SEM). Variables at different time points were compared with repeated measurement ANOVA and Bonferroni *post hoc* test. In order to compare variables between experimental groups we used two-way repeated measurement ANOVA and Dunnet *post hoc* test for multiple comparisons. To compare the maximal effects, we applied unpaired t-probe or equivalent non parametric tests. To determine the total perfusion loss area during S1P infusion, area over the curve (AOC) was calculated. All statistical analyses were performed using GraphPad Prism 7.0 and $p < 0.05$ was considered as statistically significant.

## Results

To investigate the effects of S1P on CF and cardiac function we infused $10^{-6}$ M S1P or its vehicle to the perfusate of isolated WT murine hearts for 5 min. Administration of S1P reduced CF by 44±3% (Figure 1. A). This remarkable decrease started at the beginning of the S1P infusion and continued progressively during the 5 minutes. On the wash-out period CF did not return to the control state but remained at a significantly lower value. CF reduction induced by S1P compromised left ventricular contractile performance which is evidenced by a 54±9% drop of left ventricular developed pressure (LVDevP) (Figure 1. B) and decreased +dLVP/$dt_{max}$ and -dLVP/$dt_{max}$ (indices of inotropic and lusitropic function, respectively). (Figure 1. C and D). Infusion of the vehicle itself did not affect either CF or heart function.

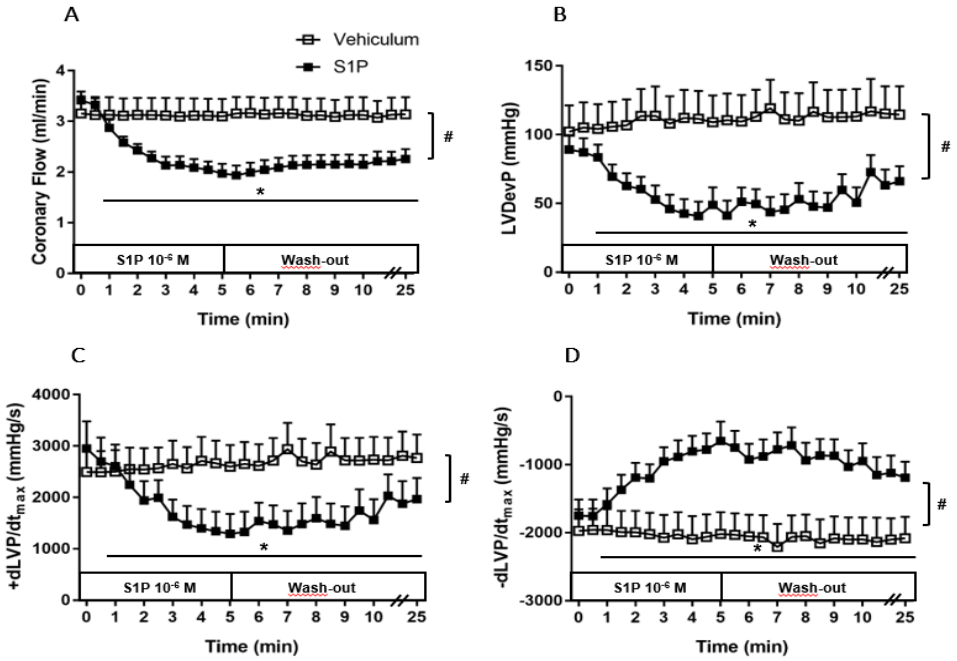


**Figure 1.** The effect of S1P on CF (panel A), LVDevP (panel B), +dLVP/$dt_{max}$ (panel C) and dLVP/$dt_{max}$ (panel D) of isolated mouse hearts. S1P ($10^{-6}$ M) or vehicle was infused to the perfusate of isolated WT murine hearts for 5 minutes. The infusion period was followed by a 20-minute wash-out period. Administration of S1P resulted in a remarkable decrease in CF which prevailed throughout the infusion and the wash-out period. CF reduction compromised left ventricular contractile performance as evidenced by a concomitant decrease in LVDevP, +dLVP/$dt_{max}$ and -dLVP/$dt_{max}$.
Mean ± SEM; n=6,9;
*$p$<0.05 vs. baseline (pre-infusion value), repeated measurement ANOVA followed by Dunnett's *post hoc* test;
#$p$<0.05 vs. vehicle; two-way repeated measurement ANOVA and Dunnett's multiple comparisons test.

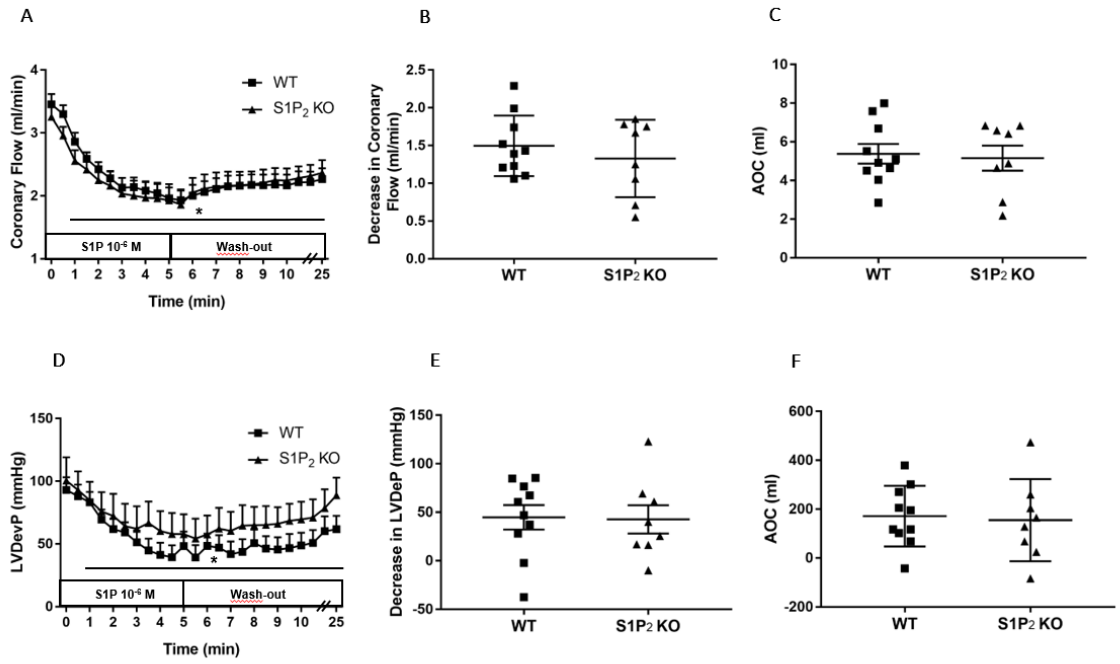


**Figure 2.** The effect of S1P on CF (Panel A-C) and LVDevP(Panel D-F) in hearts isolated from WT and $S1P_2$ KO mice. S1P ($10^{-6}$ M) was infused to the perfusate of isolated WT and $S1P_3$ KO murine hearts for 5 min. The infusion period was followed by a 20-minute wash-out period. CF and LVDevP are illustrated on Panel A and D during the whole protocol. Maximal decrease in CF and LVDevP compared to baseline (preinfusion) are shown on Panel B and E. The area over the curve (AOC) are illustrated on Panel C and F. In $S1P_2$ deficient hearts the S1P induced CF and LVDevP reduction was similar to the WT mice.
Mean ± SEM; n=10, 8;
**p*<0.05 vs. baseline (preinfusion value), repeated measurement ANOVA followed by Dunnet's *post hoc* test;
#*p*<0.05 vs. vehiculum; two-way repeated measurement ANOVA and Dunnett's multiple comparisons test; unpaired t-test.

In $S1P_3$ KO hearts the CF reducing effect of S1P was significantly diminished compared to WT mice (Figure 3. Panel A). There was a remarkable difference in the maximal effects as well. CF was dropped by 1.95±0.33 ml/min in WT and only by 0.93±0.10 ml/min in $S1P_3$ KO mice (Figure 3. Panel B). Area over the curve used as an index for total perfusion loss during the infusion period showed similar results. During the 5-minute-long S1P infusion the total perfusion loss was 8.56±1.6 ml in WT vs. 3.70±0.57 ml in $S1P_3$ KO mice (Figure 3. Panel C).

The decrease in left ventricular contractile performance upon S1P infusion was also moderated in $S1P_3$ KO mice: the drop in LVDevP (Figure 3. Panel D-E), and area over the LVDevP curve used as a measure of loss of contractile activity (Figure 3. Panel F) were significantly smaller compared to controls.

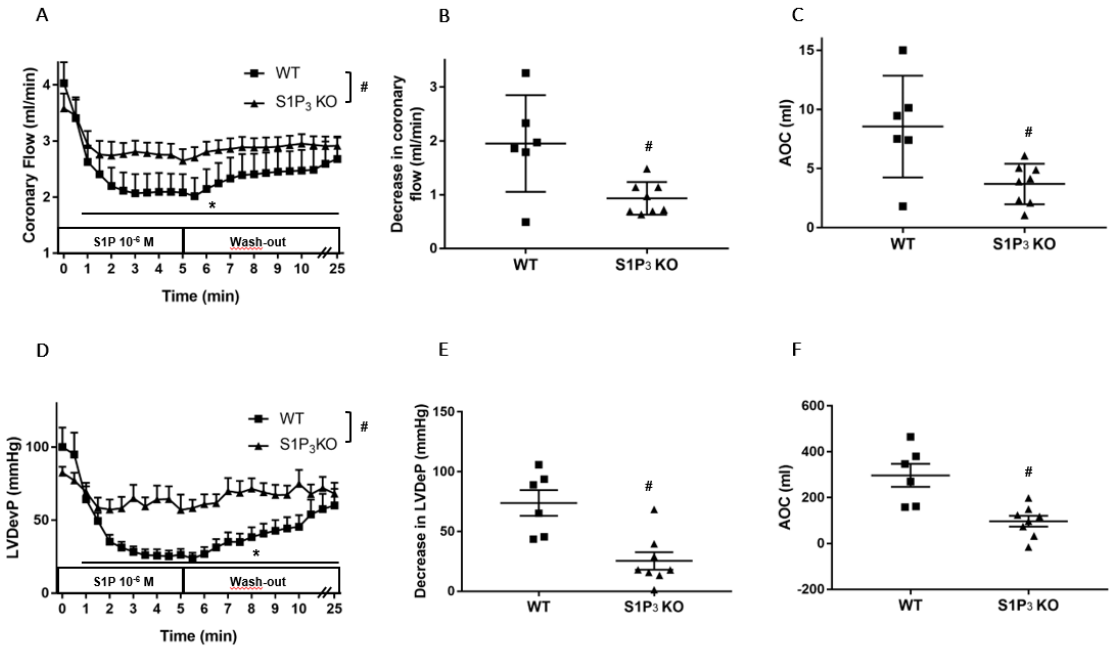


**Figure 3.** The effect of S1P on CF (Panel A-C) and LVDevP (Panel D-F) in hearts isolated from WT and $S1P_3$ KO mice. S1P ($10^{-6}$ M) was infused to the perfusate of isolated WT and $S1P_3$ KO murine hearts for 5 min. The infusion period was followed by a 20-minute wash-out period. CF and LVDevP are illustrated on Panel A and D during the whole protocol. Maximal decrease in CF and LVDevP compared to baseline (preinfusion) are shown on Panel B and E. The area over the curve (AOC) are illustrated on Panel C and F. In $S1P_3$ deficient hearts the S1P induced coronary flow and LVDevP reduction was significantly diminished.
Mean ± SEM; n=6, 8;
*$p$<0.05 vs. baseline (preinfusion value), repeated measurement ANOVA followed by Dunnet's *post hoc* test;
#$p$<0.05 vs. vehiculum; two-way repeated measurement ANOVA and Dunnett's multiple comparisons test; unpaired t-test.

To solve the contradiction between the well-known cardioptotective and observed cardiac function reducing effect of S1P we aimed to separate the role of "endogenous" (derived from myocardium) and "exogenous" (derived from vessel) S1P.
Firstly, we investigated the role of "endogenous S1P". Instead of S1P pretreatment, its vehicle was infused to the perfusion solution either to WT and $S1P_3$ KO hearts (Figure 4. Column 1). CF during the reperfusion period did not differ significantly in the two groups (Figure 4. Panel A/1). On the contrary, parameters representig cardiac function did remarkably show difference. Loss of the $S1P_3$ receptor resulted in a far worse recovery of the cardiac funtion (Figure 4. Panel B/1-E/1).
Secondly, we investigated the role of "exogenous S1P". S1P pretreatment was carried out by infusing S1P to the perfuison solution before ischaemia at a concentration of $10^{-6}$ M for 5 minutes. (Figure 4. Coloumn 2).
During the reperfusion period CF returned to a significantly higher value in the $S1P_3$ KO hearts (Figure 4. Panel A/2). On the other hand, recovery of the cardiac function did not differ remarkably in the two groups (Figure 4. Panel B/2-E/2).
Lastly, we compared the postischaemic recovery of the S1P pretreated groups (Figure 4. Colomn 2) and the groups infunded with only vehicle prior to I/R (Figure 4, Column 1). Preischemic S1P treatment worsened the recovery of either CF and contractile function both in WT and $S1P_3$ KO hearts.

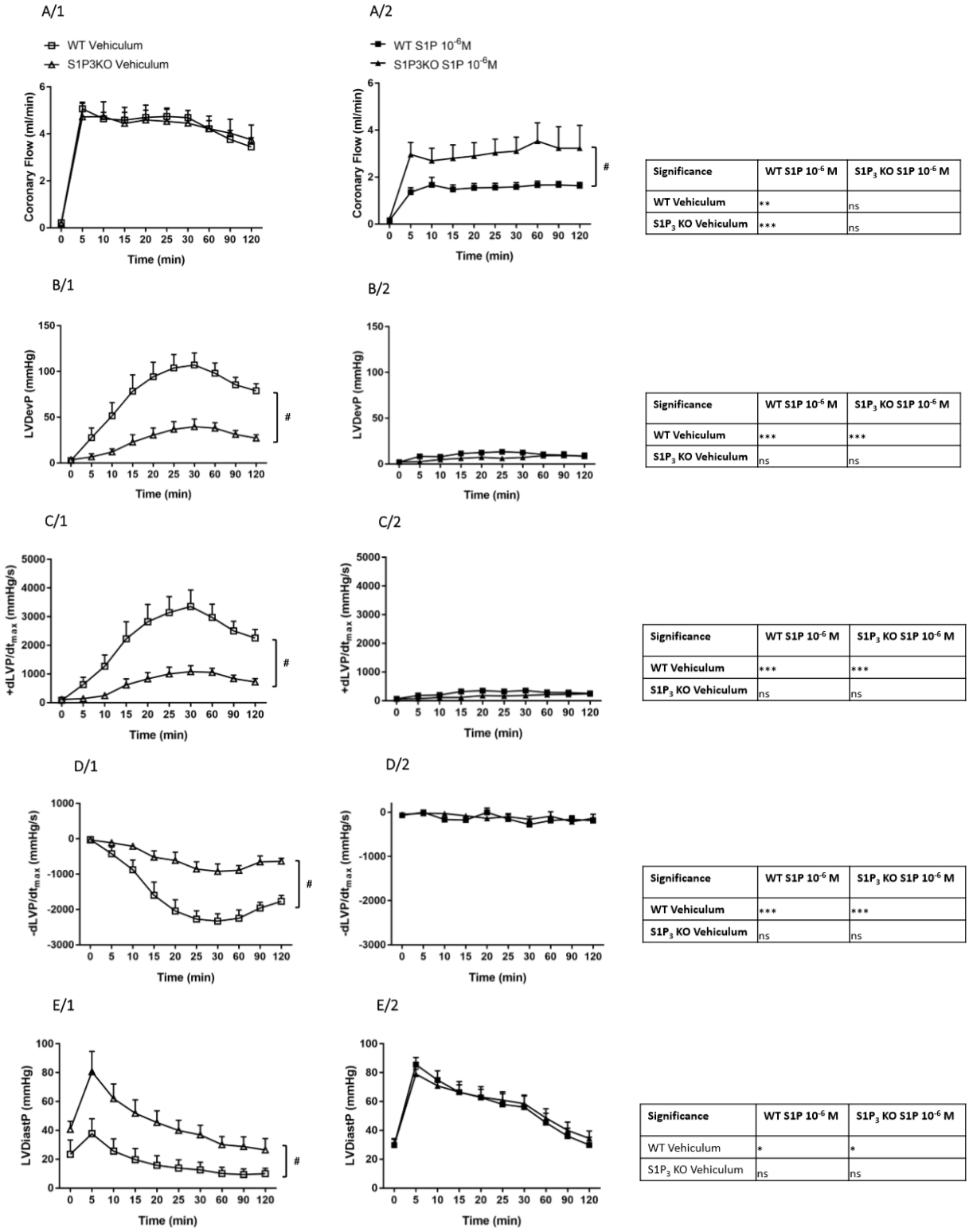


| Significance | WT S1P $10^{-6}$ M | $S1P_3$ KO S1P $10^{-6}$ M |
|---|---|---|
| WT Vehiculum | ** | ns |
| $S1P_3$ KO Vehiculum | *** | ns |

| Significance | WT S1P $10^{-6}$ M | $S1P_3$ KO S1P $10^{-6}$ M |
|---|---|---|
| WT Vehiculum | *** | *** |
| $S1P_3$ KO Vehiculum | ns | ns |

| Significance | WT S1P $10^{-6}$ M | $S1P_3$ KO S1P $10^{-6}$ M |
|---|---|---|
| WT Vehiculum | *** | *** |
| $S1P_3$ KO Vehiculum | ns | ns |

| Significance | WT S1P $10^{-6}$ M | $S1P_3$ KO S1P $10^{-6}$ M |
|---|---|---|
| WT Vehiculum | *** | *** |
| $S1P_3$ KO Vehiculum | ns | ns |

| Significance | WT S1P $10^{-6}$ M | $S1P_3$ KO S1P $10^{-6}$ M |
|---|---|---|
| WT Vehiculum | * | * |
| $S1P_3$ KO Vehiculum | ns | ns |

**Figure 4.** The effect of I/R on CF (panel A), LVDevP (panel B), +dPdtmax (panel C), -dPdtmax (panel D) and left ventricle diastolic pressure (panel E) of isolated WT and $S1P_3$ KO mouse hearts. Vehicle (Coloumn 1) or S1P (Coloumn 2) was infused to the perfusate of isolated murine hearts at a concentration of $10^{-6}$ M. The infusion period was maintained for 5 minutes which was followed by a 20-minute-long global ischaemia and 120 minutes reperfusion period. On panel A-E reperfusion period is illustrated.
Mean ± SEM; n=6,8,7,7;
#$p<0.05$ vs. $S1P_3$ KO; two-way repeated measurement ANOVA on ranks and Dunn's multiple comparisons test

Along with those results presented above relative infarct size was also larger in $S1P_3$ KO (10,72±2,93%) than in WT (1,12±0,37%) hearts (Figure 5. Panel A/1-B/1) in the vehicle pretreated groups. In S1P pretreated groups infarct size (Figure 5. Panel A/2-B/2) did not differ remarkably between $S1P_3$ KO and WT hearts.
Comparing the size of the infarcted area of the S1P pretreated groups (Figure 5. Panel A/2-B/2) and the groups infunded with only vehicle prior to I/R (Figure 5. Panel A/1-B/1) preischemic S1P treatment increased relative infarct size.

Most studies identifying cardioprotection choose relative infarct size as outcome. LVDevP as a representative parameter of the heart function is rarely investigated. We aimed to compare these two parameters. Relative infarct size was correlated to LVDevP at the 120$^{th}$ minute of the reperfusion period. We found a strong correlation (r=-0,7371) between the two parameters (Figure 5, Panel C).

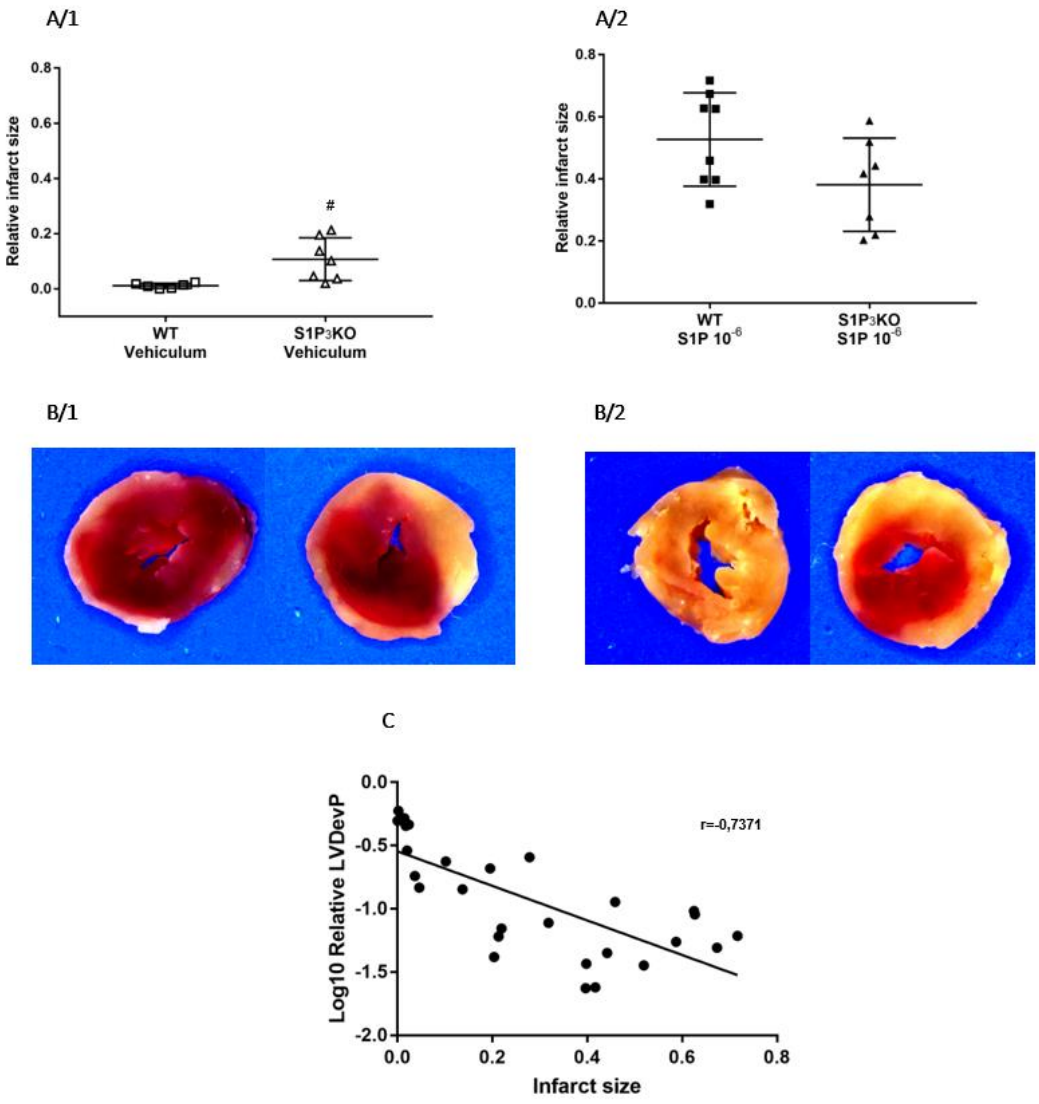


**Figure 5.**
Relative infarct size (Panel A) and representative sections from hearts (Panel B) calculated and captured after reperfisuion. In the second column S1P pretreatment was applied. Relative infarct size was correlated to relative LVDevP at the 120$^{th}$ minute of the reperfusion period. (Panel C).
Mean ± SEM; n=6,8,7,7;
#p<0.05 vs. $S1P_3$ KO, unpaired t-test (Panel A), Pearson's correlation (Panel C)

## Discussion

In the present *ex vivo* study we characterized the complex effects of ischemia related exposition of the heart to S1P via the coronary system. We observed that preischemic administration of S1P to the coronary circulation reduces coronary flow and diminishes cardiac contractile performance. In our experiments, the hemodynamic restitution of S1P pretreated hearts after non-fatal global ischemia was poor compared to that of control hearts, moreover S1P aggravated myocardial tissue damage. Using an S1P3 gene-deficient mouse model we could show that this receptor mediates cardioprotection against ischemia/reperfusion injury, but this beneficial effect is abolished by preischemic S1P administration.

The major sources of plasma S1P are red blood cells and platelets. Sphingosine kinase (SPHK) is highly active in platelets and synthesizes S1P from sphingosin taken up from the plasma and produced at the outer leaflet of the platelet membrane. Platelets store S1P abundantly and release it upon activation. In acute coronary syndrome, when blood clotting is activated by the rupture of an atherosclerotic plaque a substantial amount of S1P may be released to the circulation. S1P has been reported to have vasoconstrictor and endothelium-dependent vasodilator actions in various vascular beds. However, despite its potential pathophysiological relevance, only few studies investigated the effects of S1P on the coronaries, and none of them attempted to relate it to contractile activity. The first aim of our study was to mimic massive S1P exposure of the heart which may occur in ACS upon platelet activation and explore its effects on coronary perfusion and heart function. For this purpose, we administered S1P to the coronary perfusate of isolated murine hearts. This produced a remarkable decrease in coronary flow (Fig. 1A). This observation is in agreement with earlier studies which also ascribed vasoconstrictor effects to S1P in coronaries and other vascular beds. (14)(13) Murakami *et al* reported dose-dependent S1P-induced coronary flow reduction in rat hearts in a similar experimental setting. (13) The S1P induced flow deprivation in our study was associated with serious decline in cardiac performance, which was evidenced by decreased LVDevP, +dLVP/dtmax and - dLVP/dtmax (Fig. 1 B-D). This may be primarily attributed to CF reduction. However, direct negative inotropic effect of S1P on cardiomyocytes reported by earlier studies may also play a role. (15)(16)

The cellular actions of S1P are ascribed to the presence of five specific G-protein coupled S1P receptors, $S1P_1$ to $S1P_5$. (22) From these, $S1P_1$, $S1P_2$ and $S1P_3$ receptors are expressed abundantly in the CV system. (23) Detailed description of S1P signaling in coronaries is not available in the literature, however some studies provide evidence that $S1P_2$ and $S1P_3$ may play a role. Therefore, we aimed to characterize the role of these 2 receptors in the observed coronary flow reducing effect of S1P. Using an S1P3 receptor gene-deficient mouse model, we showed that $S1P_3$ receptor plays the most relevant role in the signaling of S1P-induced CF reduction, as absence of this receptor diminishes significantly the CF reducing effect of S1P (Fig. 2C). This observation confirms the findings of Murakami *et al.* who raised the role of S1P3 in coronary constriction using the S1P3 receptor inhibitor, TY-52156 in a similar experimental setting (13). Other investigators proposed the participation of $S1P_2$ receptors, as they observed S1P induced constriction in human coronary smooth muscle cells, which was attenuated by the $S1P_2$ inhibitor, JTE-013 (14). However, our *ex vivo* experiments in which we used $S1P_2$ receptor deficient mice did not verify these findings. This does not necessarily mean that $S1P_2$ receptor does not have a role in the regulation of coronary vessel tone, it might be that $S1P_2$-related endothelium-dependent vasodilator, and direct vasoconstrictor effects on smooth muscle cells neutralize each other in our experiments.

S1P is frequently related to cardioprotection. Indeed, numerous studies have shown that it decreases the infarcted area and apoptotic cell death after ischemia-reperfusion injury, and that it plays a role in the mechanism of ischemic pre- and postconditioning. (6)(7)(8)(9)10,11, 12 . Concerning signaling, participation of S1P2 and S1P3 receptors has been suggested. However, presence of this protective effect has been concluded from experiments using fundamentally different methodological approaches. In most studies, inhibition of S1P signaling (by using S1P gene-deficient models or inhibition of SphK1 and SphK2 enzymes) was applied in ischemia, which made ischemic/reperfusion injury more severe and reduced the benefits of ischemic pre- and postconditioning. These suggest that S1P signaling is stimulated in ischemia most probably by locally derived 'endogenous' S1P, released from the tissues of the heart. The other approach applies S1P administration into blood circulation ('exogenous' S1P) before the ischemic insult. Although, this experimental setting can be considered as a good model for S1P release in ACS, only few investigators explored S1P effects this way, and they only assessed tissue damage without addressing the influence of S1P on postischemic heart function. Anyway, these studies also reported a decrease in infarcted area (12, 14), which is somewhat surprising if we consider that S1P has several short-term effects in the heart (i.e. coronary flow reduction, negative inotropy) that may be detrimental to postischemic contractile recovery. Our current study was designed to combine these approaches in the context of S1P3 receptor signalling. Our choice to focus on S1P3 receptor signalling was motivated by the results of our experiments presented in Figure 2 and 3, which highlight that short-term S1P cardiac effects are mediated by S1P3 in large part, however, S1P2 (the other receptor proposed to participate in cardioprotection) does not have a major role.

Firstly, we aimed to clarify whether intrinsic activation of S1P3 signalling during ischemia is protective in our experimental setting. Our results showed that in the absence of S1P3, murine hearts were more susceptible to a 20-min-long global ischemic insult. This was evidenced by weaker contractile recovery during the 2 hour reperfusion period (Figure 4 B/1-D/1), higher postischemic end-diastolic pressure (Figure 4 E/1) demonstrating more severe myocardial contracture, and larger infarct size (Figure 5 A/1 and B/1). This severe functional and morphological injury developed despite a relatively sufficient coronary flow which approached the preischemic value and was not worse than that of wild type hearts during the reperfusion period (Figure 4 A/1). These observations not only confirmed the protective effect of S1P3 signalling of earlier investigations which reported larger infarct size in S1P3 KO hearts, but also extended cardioprotection to postischemic cardiac functionality.

In our study we investigated the effects of S1P on ischemia/reperfusion injury also by the other methodological approach described in literature, namely by using an experimental setting where S1P is administered to the coronary circulation before ischemia. Preischemic S1P infusion can be considered as simulation of S1P release in ACS. After S1P pretreatment, we applied a non-fatal ischemia protocol and followed up recovery of cardiac function upon reperfusion. These experiments explored S1P effects more broadly than previous investigations. Beyond the determination of infarct size, we also assessed postischemic cardiac function. We found that preischemic S1P was not only deleterious during infusion, but it also aggravated ischemic injury. After an ischemic insult which is supposed to be non-fatal, the infarcted tissue constituted large part of the myocardium, and restitution of contractile activity was hardly observable in WT hearts. The latter was evidenced by extremely low LVDevP, +dLVP/dtmax and - dLVP/dtmax values (Figure 4.) which failed to approach preischemic levels during reperfusion, although coronary flow recovered relatively well. Comparing ischemic injury of S1P pretreated and non-treated WT hearts, infarct size was significantly larger, whereas LVDevP, +dLVP/dtmax and - dLVP/dtmax values were significantly lower at the end of the 2-

h reperfusion period. Our results contradict the observations of other researchers who observed decreased infarct size after preischemic S1P treatment. This difference may be explained by differences in methodology. Anyway, we believe our results are more in line with our expectations which rely on the fact that pre ischemic S1P infusion impairs coronary flow and pump function.

As we had observed that the coronary effects of S1P are in part mediated by S1P3 receptors (Figure 3.), we also explored the effects of preischemic S1P infusion on ischemic damage in S1P3 KO hearts. Although the preischemic CF and function of S1P3 KO hearts were better (data not shown, we refer to the data in Figure 3.), their functional recovery was as weak, and infarct size as large as that of WT hearts. Interestingly, although CF in S1P3KO hearts returned to the preischemic value, this relatively better perfusion did not pose any benefit for cardiac performance.

•

•

•

•

•

•

•

## Conclusion

In this study, using isolated perfused murine hearts we designed an experimental model to simulate S1P release during thrombus formation in acute coronary syndrome. We described the complex effects of preischemic intracoronary administration of S1P on heart function, postischemic functional recovery and tissue survival. S1P treatment caused a substantial decrease in coronary flow and heart function. Using gene-deficient animal models, we proved $S1P_2$ receptor have minor role in this effect, whereas $S1P_3$ receptor is a key factor in signaling. The postischemic functional recovery was more depressed, and the ratio of infarcted area was more enhanced in S1P pretreated hearts. Preischemic S1P treatment also abolished the cardioprotective effects mediated by S1P3 receptors. These findings highlight that in clinical situations when thrombotic coronary occlusion causes cardiac ischemia, the released S1P may compromise postischemic recovery due to its unfavorable effects on heart function and may outweigh the widely-reported cardioprotective effects of S1P produced by the ischemic myocardium.

## Acknowledgements

This research was funded by the OTKA 112964 grant.

# Reference


1. Makki N, Brennan TM, Girotra S. Acute coronary syndrome. J Intensive Care Med. 2015;30(4):186–200.
2. Tsai HC, Han MH. Sphingosine-1-Phosphate (S1P) and S1P Signaling Pathway: Therapeutic Targets in Autoimmunity and Inflammation. Drugs. 2016;76(11):1067–79.
3. Wang G, Bieberich E. Sphingolipids in neurodegeneration (with focus on ceramide and S1P). Adv Biol Regul [Internet]. 2018;70:51–64. Available from: https://doi.org/10.1016/j.jbior.2018.09.013
4. Yatomi Y, Ruan F, Hakomori SI, Igarashi Y. Sphingosine-1-phosphate: A platelet-activating sphingolipid released from agonist-stimulated human platelets. Blood. 1995;86(1):193–202.
5. Peters SL, Alewijnse AE. Sphingosine-1-phosphate signaling in the cardiovascular system. Curr Opin Pharmacol. 2007;7(2):186–92.
6. Igarashi J, Michel T. Sphingosine-1-phosphate and modulation of vascular tone. Cardiovasc Res. 2009;82(2):212–20.
7. Siess W. Athero- and thrombogenic actions of lysophosphatidic acid and sphingosine-1-phosphate. Biochim Biophys Acta - Mol Cell Biol Lipids. 2002;1582(1–3):204–15.
8. Mutoh T, Rivera R, Chun J. Insights into the pharmacological relevance of lysophospholipid. 2012;
9. Tigyi GJ. Lysophospholipid Receptors. Encyclopedia of Biological Chemistry: Second Edition. 2013. 762-764 p.
10. Karliner JS. Sphingosine kinase and sphingosine 1-phosphate in the heart: A decade of progress. Biochim Biophys Acta - Mol Cell Biol Lipids [Internet]. 2013;1831(1):203–12. Available from: http://dx.doi.org/10.1016/j.bbalip.2012.06.006
11. Jin ZQ, Goetzl EJ, Karliner JS. Sphingosine kinase activation mediates ischemic preconditioning in murine heart. Circulation. 2004;110(14):1980–9.
12. Vessey DA, Kelley M, Li L, Huang Y, Zhou HZ, Bo QZ, et al. Role of sphingosine kinase activity in protection of heart against ischemia reperfusion injury. Med Sci Monit. 2006;12(10):318–24.
13. Means CK, Xiao CY, Li Z, Zhang T, Omens JH, Ishii I, et al. Sphingosine 1-phosphate S1P2 and S1P3 receptor-mediated Akt activation protects against in vivo myocardial ischemia-reperfusion injury. Am J Physiol - Hear Circ Physiol. 2007;292(6).
14. Theilmeier G, Schmidt C, Herrmann J, Keul P, Schäfers M, Herrgott I, et al. High-density lipoproteins and their constituent, sphingosine-1-phosphate, directly protect the heart against ischemia/reperfusion injury in vivo via the S1P3 lysophospholipid receptor. Circulation. 2006;114(13):1403–9.
15. Murakami A, Takasugi H, Ohnuma S, Koide Y, Sakurai A, Takeda S, et al. Sphingosine 1-phosphate (S1P) regulates vascular contraction via S1P 3 receptor: Investigation based on a new S1P3 receptor antagonist. Mol Pharmacol. 2010;77(4):704–13.
16. Ohmori T, Yatomi Y, Osada M, Kazama F, Takafuta T, Ikeda H, et al. Sphingosine 1-phosphate induces contraction of coronary artery smooth muscle cells via S1P2. Cardiovasc Res. 2003;58(1):170–7.

17. Means CK, Miyamoto S, Chun J, Brown JH. S1P1 receptor localization confers selectivity for G i-mediated cAMP and contractile responses. J Biol Chem. 2008;283(18):11954–63.

18. Landeen LK, Dederko DA, Kondo CS, Hu BS, Aroonsakool N, Haga JH, et al. Mechanisms of the negative inotropic effects of sphingosine-1-phosphate on adult mouse ventricular myocytes. Am J Physiol Circ Physiol. 2008;294(2):H736–49.

19. Sanna MG, Liao J, Jo E, Alfonso C, Ahn MY, Peterson MS, et al. Sphingosine 1-Phosphate (S1P) Receptor Subtypes S1P1 and S1P3, Respectively, Regulate Lymphocyte Recirculation and Heart Rate. J Biol Chem. 2004;279(14):13839–48.

20. Forrest M, Sun SY, Hajdu R, Bergstrom J, Card D, Doherty G, et al. Immune Cell Regulation and Cardiovascular Effects of Sphingosine 1-Phosphate Receptor Agonists in Rodents Are Mediated via Distinct Receptor Subtypes. J Pharmacol Exp Ther. 2004;309(2):758–68.

21. Skrzypiec-Spring M, Grotthus B, Szelag A, Schulz R. Isolated heart perfusion according to Langendorff-Still viable in the new millennium. J Pharmacol Toxicol Methods. 2007;55(2):113–26.

22. NACHLAS MM, SHNITKA TK. Macroscopic identification of early myocardial infarcts by alterations in dehydrogenase activity. Am J Pathol. 1963;42(4):379–405.

**Classification:** BIOLOGICAL SCIENCES, Biochemistry

# SPHINGOSINE INHIBITS CALMODULIN ACTION: IMPLICATION FOR REGULATION OF ENDOTHELIAL NITRIC OXIDE SYNTHASE-MEDIATED VASORELAXATION

Tünde Juhász[a], Éva Ruisanchez[b], Veronika Harmat[c,d], József Kardos[e], Mónika Kabai[x] Viktor Erdősi[b] Zoltán Benyó[b], Károly Liliom[f]

[a]Institute of Materials and Environmental Chemistry, Research Centre for Natural Sciences, Hungarian Academy of Sciences, Magyar Tudósok krt. 2, Budapest, H-1117 Hungary
[b]Institute of Translational Medicine, Semmelweis University, Tűzoltó u. 37–47, H-1094 Budapest, Hungary
[c]Laboratory of Structural Chemistry and Biology, Institute of Chemistry, Eötvös Loránd University, Pázmány Péter sétány 1/A, H-1117 Budapest, Hungary
[c]Protein Modelling Research Group, Hungarian Academy of Sciences - Eötvös Loránd University, Pázmány Péter sétány 1/A, H-1117 Budapest, Hungary
[e]Department of Biochemistry, Eötvös Loránd University, Pázmány Péter sétány 1/C, H-1117 Budapest, Hungary
[f]Department of Biophysics and Radiation Biology, Semmelweis University, Tűzoltó u 37-47, Budapest, H-1094 Hungary,

**To whom correspondence should be addressed:**
Károly Liliom
Tel.: +36 30 8246229
Email: liliom.karoly@med.semmelweis-univ.hu

## Abstract

Calmodulin (CaM), the main modulator in calcium signaling, regulate the function of a great number of proteins. The signaling lipid Sph has been reported to inhibit several CaM-dependent enzymes, and we hypothesized that Sph can directly bind to CaM. Here we characterize the interaction of CaM with Sph and its functional effects. *in vitro* binding assays revealing that Sph binds to both apo and $Ca^{2+}$-saturated CaM in a concentration and stoichiometry dependent manner. The presented crystal structure of the Sph-$Ca^{2+}$CaM complex gains insight into the structural basis of the interaction. We demonstrate in *in vitro* experiments that Sph was able to displace the model CaM-binding domain melittin from CaM, and to inhibit the CaM-dependent activity of the target enzymes nitric oxide synthase (NOS) and myosine light chain kinase (MLCK) regulating the vascular tone. We show that in *ex vivo* conditions, accumulation of Sph results in reduced NOS-dependent vasorelaxation, presumably due to the inhibition of CaM by Sph. Sphingolipid analogues like dimethyl- and dihydro-Sph showed similar effects in both *in vitro* and *ex vivo* assays. We conclude that the mediator lipid Sph and their analogues present/formed endogenously in eukaryotic cells might regulate CaM function, and might contribute to the control of the vascular tone *in vivo*.
211/250

## Significance Statement

The protein calmodulin (CaM), the key regulator in signaling processes using calcium ions, modulates the function of a great variety of proteins. Its function is based on its ability to bind calcium ions, upon which it undergoes conformational changes allowing it to act in a calcium-dependent manner. Up to date, the calcium ion is the only known endogenous species being able to bind to CaM and to control CaM function directly. Here we report that the lipid mediator sphingosine and their dihydro- and dimethyl analogues, formed endogenously upon enzyme activation in signaling processes, are able to bind directly to CaM independently of calcium ions. We characterize their interaction and show evidences for its functional effects as well. 117/120

\body

## Introduction

Calmodulin (CaM), the ubiquitous intracellular $Ca^{2+}$ sensor of eukaryotic cell, functions in the control of a wide variety of signaling events regulating the activity of a great number of proteins, including kinases, phosphatases, and ion channels, in a calcium-dependent manner. It is a small (148 as), evolutionary conserved protein built up of homologous N- and C-terminal globular domains connected by a flexible central linker. Both lobes are composed of two EF hand motives, allowing the binding of maximal four $Ca^{2+}$ ions [1]. $Ca^{2+}$ binding results in conformational change leading to exposure of hydrophobic patches [2], opening binding pockets for basic amphipathic helices of its target enzymes [3]. There are several small, synthetic molecules as well as natural substances with known anti-CaM activity mostly isolated from fungi and plants [4], all occupying the same target peptide binding site. However, several proteins can also bind to CaM at low Ca concentrations or independently of calcium.

Previously we have demonstrated a novel type of regulation of CaM, in which the signaling lipid sphingosylphosphorylcholine (SPC) could inhibit CaM activity directly both in the presence and the absence of calcium ions *in vitro* [5-7]. Structurally similar lysophospholipid mediators such as sphingosine-1-phosphate (S1P), lysophosphatidylcholine (LPC) and lysophosphatidic acid (LPA) showed no effect [6]. However, CaM could presumably bind to sphingosine, the structurally simplest sphingolipid (Sph) since Sph shares the basic amphipathic character of the target peptides, bearing a hydrophobic tail and a positively charged headgroup. The reported ability of Sph to inhibit several CaM-dependent enzymes [8-10] might easily be due to inhibition of CaM itself by Sph. The metabolism and action of Sph is well-studied/known. Sph is involved in apoptotic cell responses and growth arrest (for review see [11,12]), and suggested/reported to exert vasoactive effects [13,14], however, this activity has not been characterized in detail yet. Sph is formed by the action of ceramidases from ceramide, a major component of the cell membrane or by S1P-phosphatase from S1P, a signaling lipid with mostly opponent cellular effects. Sph analogues dihydro-Sph (DHS) and dimethyl-Sph (DMS) were also reported to have vasoactive properties, and to inhibit sphingosine kinase, thereby emerging as anti-cancer agents. Nevertheless, most of the studies dealing with the modulation of the vascular tone focused on the role of ceramide and S1P (i. e. the so-called "ceramide/S1P rheostat") whilst the involvement of the intermedier species Sph is not so well-documented. [15,16].

In the present study, structural and functional aspects of the interaction of CaM with Sph, and their analogues were examined. Binding assays utilizing fluorescence spectroscopy, and isothermal titration calorimetry revealed that Sph binds to both apo and $Ca^{2+}$-saturated CaM in a concentration and stoichiometry dependent manner. The presented crystal structure of the Sph-$Ca^{2+}$CaM complex shows the structural basis of a competitive inhibition at higher protein to lipid ratios. We demonstrate in *in vitro* measurements that Sph is able to dissociate the model CaM-binding domain melittin from CaM, and inhibit the CaM-dependent activity of several target enzymes phosphodiesterase, calcineurin, myosin light chain kinase, and nitric oxide synthase. Moreover, results obtained under *ex vivo* conditions point to the fact that accumulation of Sph results in reduced vasodilatation, which can easily be explained by

decreased nitric oxid synthase activity caused by inhibition of CaM by Sph. Summarized, here we report for the first time that a lipid mediator present endogenously in eukaryotic cells might directly regulate CaM function. Findings with Sph analogues point to similar effects exerted bycould exert similar effect than that of Sph.

## Results

### Sph binds to CaM in a concentration dependent manner

To test whether Sph interacts directly with CaM, binding assays were performed exploiting dansyl-CaM (dCaM) fluorescence (Fig. 1). Changes in the fluorescence properties of dCaM have been widely used to detect binding of small molecule inhibitors or target peptides of CaM, where the spectral changes could be attributed to a structural change to a collapsed CaCaM conformation allowing the protein to wrap around the binding partner(s). Similarly, addition of 100 μM Sph resulted in remarkable changes for apo- as well as $Ca^{2+}$CaM (Fig. 1A). In both cases, an increase in the fluorescence intensity of dCaM by a factor of about 2-2.5, and a shift to emission wavelength of 495-500 nm were observed in the presence of the lipid.

Measuring the effect as a function of the lipid concentration, titration of apoCaM with Sph resulted in a maximum curve (Fig. 1B), characterized by a remarkable increase in the 3-40 μM concentration range followed by a slighter decrease above 40 μM Sph. At these high lipid concentrations, a decrease in fluorescence with time was also observed, which converted the simple saturation curve to a bell-shaped one. Using CaCaM, an even more complex titration curve indicating three binding processes could be measured (Fig. 1B). Concretely, at Sph concentrations up to 2-3 μM an increase, followed by a decrease at 2-15 μM, and a further increase above 15 μM was observed.

To understand the binding determinants at various Sph concentrations, the knowledge of the lipid state in the aqueous solution applied is needed. The key parameter to characterize the lipid state is the critical micelle concentration (CMC), defined as a concentration above which micelles form. The CMC for Sph was determined by following the fluorescence change upon incorporation of a lipid soluble probe (ANS) into the micelle, and was estimated to be ~15 μM (Fig. 1B), which is in good agreement with previous data determined with the same method [17]. It should be noted that the same ANS binding profile was measured in the absence and the presence of $Ca^{2+}$ ions and EGTA (Fig. S1) indicating that micelle formation and disintegration are seemingly not affected by these species. Moreover, at concentrations below the CMC several monomers might also form smaller lipid associates, which might thermodynamically more favorable than water solvated single monomers.

Taken all the considerations above together, the following binding scenario might be concluded: i) both apo- and CaCaM are able to bind to Sph in its associated micelle form (>15 μM) resembling a membrane surface enriched in Sph, ii) binding of monomers possibly in form of associates of several monomers can be detected for CaCaM (<2 μM), iii) apo-CaM binding to aggregated but sub-micellar Sph (2-15 μM) is detectable as well, iv) apoCaM can change the micellar state of Sph at >40 μM.

Similar complex titration curves could be measured for the Sph analogues DHS and DMS (Fig. 1C and 1D).

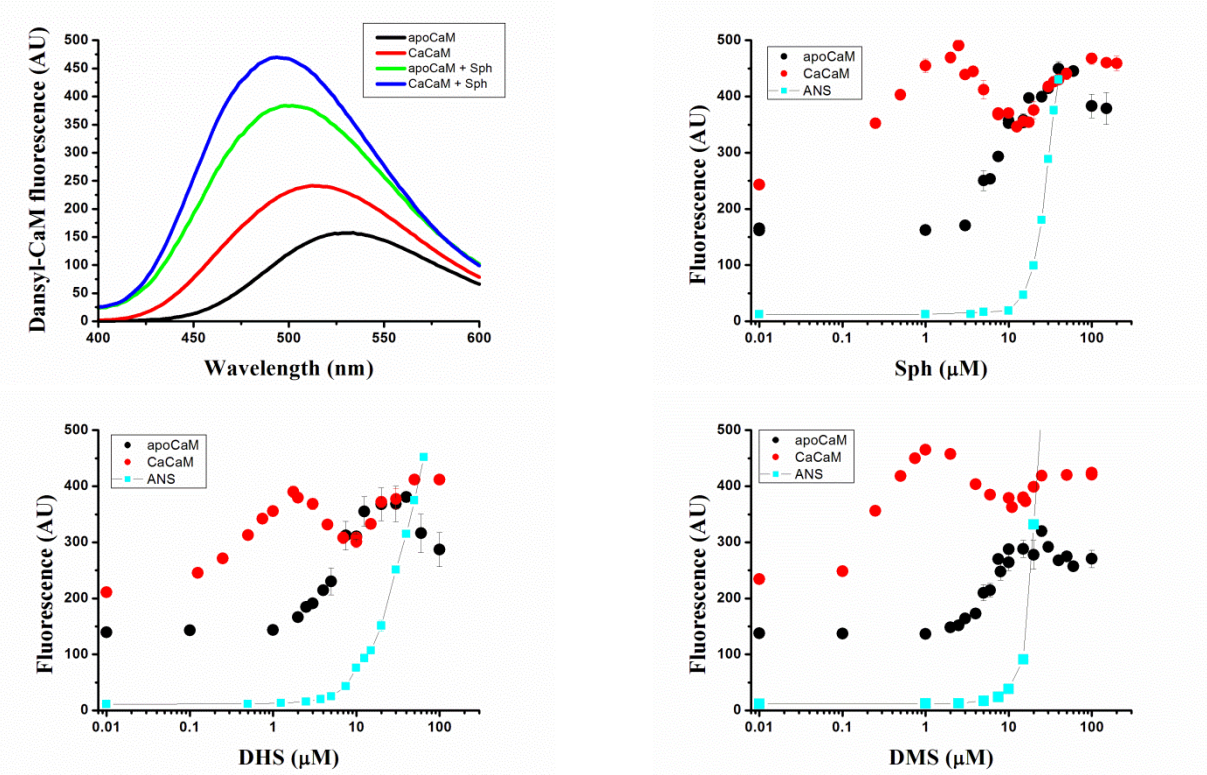


**Figure 1. Sph binds to CaM in a concentration dependent manner**

(**A**) Fluorescence spectra of dansyl-labelled apo and $Ca^{2+}$-saturated CaM (0.2 μM) in the absence and presence of 100 μM Sph (**B, C, D**) Titration of dansyl-apoCaM and dansyl-CaCaM (0.2 μM) with Sph, DMS, and DHS, respectively.

**Sph binds to CaM in a stoichiometry dependent manner**

To further examine the binding characteristics, the CaM-Sph interaction was studied utilizing ITC. Our experiments above using fluorescence spectroscopy suggested the ability of CaM to bind both lipid monomers and clusters, thus a lipid solution above the CMC, that is a mixture of monomers and micelles, was titrated with CaM. This experimental setup allowed maintaining the micellar lipid state in the cell during the titration as well as avoiding the heat effect caused by changing between the micellar and monomer lipid forms.

Titrations were performed in the presence and the absence of $Ca^{2+}$ ions. In both cases, titration data indicated two binding processes (Fig. 2A and 2B). Parameters obtained from the fitting process (Table 1) reflect the binding of one CaM molecule to one apparent binding site. In case of apoCaM, the beginning of the first process could not be resolved, thus the stoichiometry for this binding event is implicated by the estimated number of monomers forming a micelle (100-150). Taken together, similar $K_d$ values but slightly different stoichiometry values were determined for the binding processes with the apo- and the $Ca^{2+}$-saturated CaM (Table1). More concretely, the $K_d$ values for the first and second processes are in the low and the high nanomolar range (~5 nM and ~150-650 nM), respectively, while the stoichiometry values are ~5-fold smaller in the presence than in the absence of $Ca^{2+}$.

The binding events detected with Sph are very similar to those we observed previously for the CaM-SPC interaction [5]. For the latter case, we interpreted the stronger binding with higher

stoichiometry as binding of CaM to the micelle surface, while the weaker binding with lower stoichiometry as a micelle disintegration process. This could hold for the Sph-CaM interaction as well. At lower CaM to lipid ratios a few protein molecules can bind to the micelles of similar size. Upon binding of further CaMs, $Ca^{2+}$CaM could wrap around a few lipid monomers while changing its conformation into the collapsed one characteristic for target peptide binding. This binding mode was verified by the $Ca^{2+}$CaM-Sph crystal structure (see the next section). At higher apoCaM to Sph ratios, however, mixed protein-lipid micelles might form.

Considering the energetics of the CaM interactions, target peptid binding was reported to occur either entropically or enthalpically driven [18]. For the first CaM-lipid binding process, we observed positive and negative enthalpy values in the case of Sph and SPC, respectively, which indicates that binding to associated SPC could be an enthalpically but that to Sph rather an entropically driven process. According to the data, the enthalpically unfavorable nature of the reaction with Sph might be compensated by gain in entropy. It can be concluded that lipid binding like peptide binding to CaM can also be driven by different forces. As for the second binding process with Sph, small negative values were obtained for both $\Delta H$ and $-T\Delta S$ in case of $Ca^{2+}$CaM, while larger positive $\Delta H$ and negative $-T\Delta S$ values with apoCaM. Interestingly, $\Delta G$ values around −10 kcal/mol were obtained for all CaM–lipid binding processes, and similar values were reported for CaM–target peptid binding events as well [18].

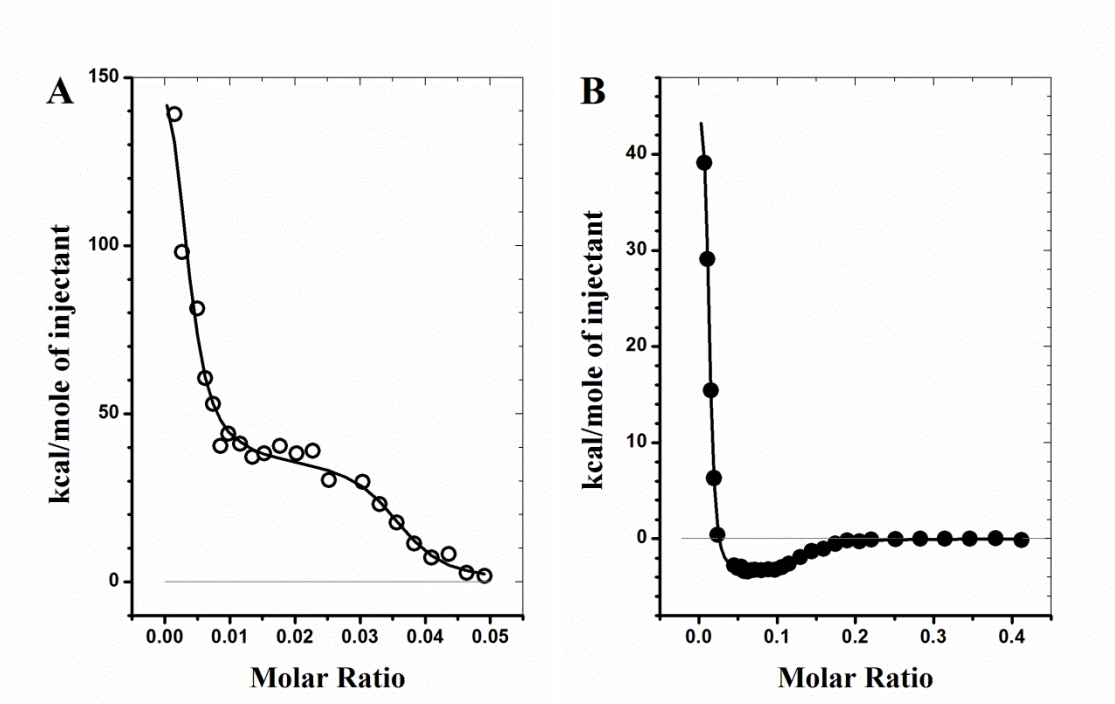


**Figure 2. Sph binds to CaM in a stoichiometry dependent manner**

Titration of Sph with CaM utilizing ITC. 200 μM Sph in the cell was titrated with 45 μM apoCaM in the presence of 100 μM EGTA (**A**), or with 400 μM $Ca^{2+}$CaM in the presence of 5 μM $Ca^{2+}$ (**B**). Parameters estimated are in Table 1.

**Table 1.** Binding parameters for the CaM-Sph interaction determined by ITC

| | | $n$ | $K_d$ | $\Delta H$ (kcal/mol) | $-T\Delta S$ (kcal/mol) |
|---|---|---|---|---|---|
| $Ca^{2+}$CaM | First process | 82 ± 1 | 6.0 ± 1.9 nM | 49 ± 1 | -60 |
| | Second process | 8 ± 0.2 | 0.64 ± 0.20 μM | −3.9 ± 0.1 | -5 |
| ApoCaM | First process | ~ 300 * | 4.2 ± 2.6 nM | 187 ± 17 | -199 |
| | Second process | 40 ± 1 | 0.13 ± 0.09 μM | 41 ± 4 | -50 |

* the stoichiometry *n* was estimated and set to 300 in the fitting process

**Crystal structure of the $Ca^{2+}$CaM/Sph complex**

Structure of $Ca^{2+}$CaM co-crystallized with Sph was solved and refined to 1.9 Å resolution (Fig. 3). The crystals are iso-structural with those of the $Ca^{2+}$CaM/SPC complex, showing CaM in collapsed overall conformation with a hydrophobic channel formed between its two domains. The structure of the $Ca^{2+}$CaM/Sph complex resembles to that of the $Ca^{2+}$CaM/SPC complex in the following characteristics: i) the hydrophobic pockets of CaM responsible for binding an anchoring residue in many complexes are open, ii) the overall conformation of CaM is well defined by electron density except for the central linker region between the two domains and the ends of the peptide chains (the structures can be aligned with RMSD of the backbone atoms being 0.310 Å, Fig. 3B), iii) partial structures of four nearly parallel ligand chains bound in the channel of CaM, and a shorter fragment of the lipid molecule at the edge of the hydrophobic channel can be recognized in electron density maps (Fig. 3B). However, there are characteristic differences between the two complexes. Though both the negatively charged residues of CaM and its hydrophobic pockets are generally thought to have important roles in ligand binding, there is no clear electron density in these regions in the $Ca^{2+}$CaM/Sph structure (Fig. 3B, and S2). The refined B-factors of the lipid chains are higher for SPC than Sph in their complexes. Assuming that the lipid chains completely fill the hydrophobic channel of CaM, this suggests that higher B-factors are caused by lower occupancy of the lipid chains in the former crystal. The fact that there is no continuous electron density of Sph in the hydrophobic pockets or near the negatively charged region of CaM surface suggests that the main difference between SPC and Sph binding is that parts of Sph molecules outside the hydrophobic channels are more disordered, lacking the orienting role of a charged head moiety.

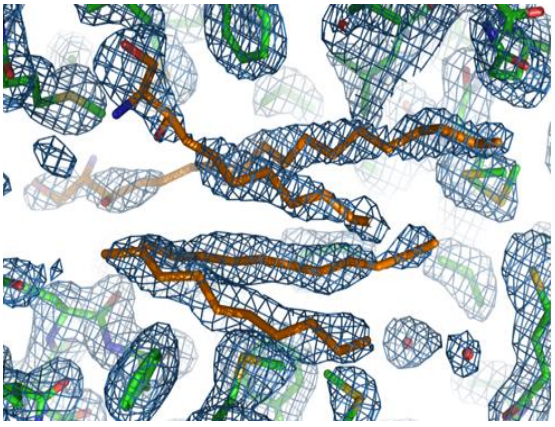

**Figure 3. Crystal structure of the $Ca^{2+}$CaM/Sph complex**

In the $Ca^{2+}$CaM/Sph complex, four Sph monomers bound in the central channel of CaM can be identified. The lipids showed lower electron density so that not all parts of the Sph molecules could be determined. (**A**) Part of the electron density map showing the bound lipids and the surrounding CaM residues. (**B**) Side view of the complex. CaM is shown in ribbon representation (from the N- to the C-terminus coloured from blue to red), and the Sph molecules are represented as magenta sticks.

**SPC dissociates the CaM–target peptide complex**

Melittin, the most abundant component of honey bee venom is widely used as the model CaM-binding domain of CaM target enzymes. Upon binding to CaM, the peptide forms a basic amphipatic helix, the typical structure of the CaM-binding domain. The melittin-CaM interaction is characterized by a dissociation constant in the low nanomolar range (reported values lie between 3 and 140 nM [7]). Our ITC measurements (see above) indicated a binding of similar strength for Sph to CaM binding to CaM, thus possible interference of Sph binding with melittin binding to CaM was investigated exploiting dansyl-CaM and melittin tryptophan fluorescence.

We have shown (see above) that Sph binding affected the fluorescence spectrum of dansyl-CaCaM in a complex way involving elevated fluorescence and a blue shift upon addition of micellar Sph. Binding of melittin resulted in even higher changes in the spectrum, causing approximately 3-fold increase in the emission intensity, and an approximately 25 nm blue shift (Fig. 4A), similarly as observed previously [6]. Addition of Sph to the melittin-CaM complex decreased the signal to the values typical for the Sph-bound spectrum (Fig. 4A). Measuring the concentration dependence of the effect, titration of the CaM-melittin complex with Sph resulted in a saturation curve yielding an apparent $K_d$ of 15 μM and a Hill-coefficient of 3.3 (Fig. 4B), which can reflect the lipid association process again. These results are consistent with dissociating the CaM-target peptide complex in the presence of Sph clusters.

In the complementer experiment exploiting melittin Trp fluorescence (Fig. 4C), the binding of melittin to CaM resulted in a red shift and an elevation in the intensity. The presence of 100 μM Sph caused no change in the melittin spectrum indicating no incorporation of the peptide into the Sph micelle. Melittin is known for its ability to integrate into lipid bilayers and micelles, however, its fairly positive character with six positively charged residues precluded contact to the Sph surface bearing positively charged amine groups. Adding melittin to CaM preincubated with Sph, a spectrum characteristic for the free peptide could be measured. In the competitive system, when CaM was added to the mixture of the non-binding partners Sph and melittin, the unbound peptide form was detected. These findings are indicative of a higher affinity of CaM to Sph associates over to melittin.

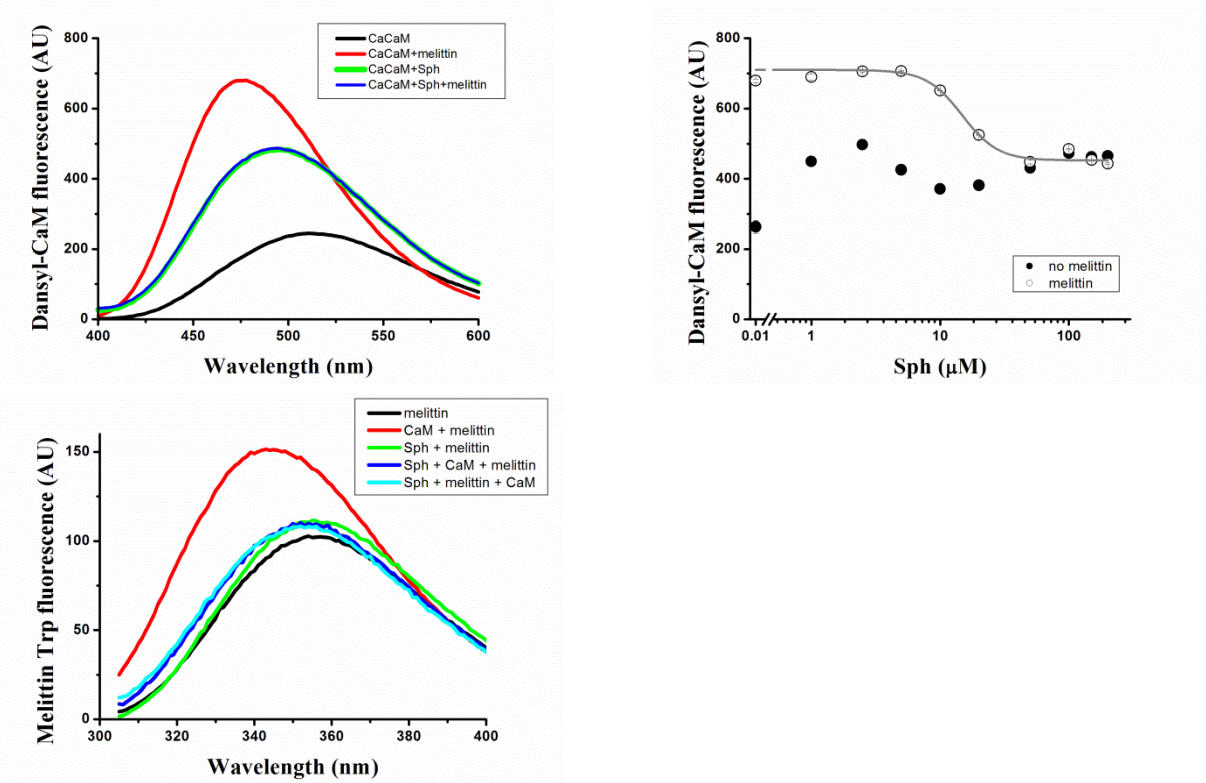


**Figure 4. Sph dissociates the CaM–target peptide complex**

(**A**) Fluorescence spectra of dansyl-labeled $Ca^{2+}$-saturated CaM (0.2 μM) in the absence and presence of 100 μM Sph and 0.4 μM melittin. (**B**) Titration of the dansyl-$Ca^{2+}$CaM (0.2 μM) with Sph in the presence of melittin (0.4 μM). The titration resulted in a saturation curve yielding an apparent $K_d$ of 15 ± 1 μM and a Hill-coefficient of 3.3 ± 0.6. (**C**) Fluorescence spectra of melittin (0.6 μM) in the absence and presence of CaCaM (1.2 μM), and Sph (100 μM).

**Sph can inhibit CaM function *in vitro***

CaM regulates many proteins, among them a high number of enzymes, following the activation of which induced by CaM offers an effective way to probe CaM function *in vitro*. The effect of Sph was studied with the widely used targets PDE, and CaN, the details of which are described in the Supplementary Information (Figures S3, and S4, and related text). Summarized, our findings suggested enzyme activating ability of CaM inhibited in the presence of associated Sph. To further clarify inhibitory potential, the effect of Sph, and its analogues on the CaM-dependent activitiy was studied using enzymes involved in controlling the vascular tone, *i. e.* the endothelial nitric oxid synthase (eNOS), and myosin light chain kinase (MLCK).

eNOS produces the neurotransmitter nitric monoxide (NO) from arginine, thereby acting as a vasodilator *in vivo*. Enzyme activity under *in vitro* conditions was tested at various CaM concentrations using 0.5 U recombinant eNOS, and an elevation of approx. 60% was measured when increasing the CaM concentration from 0.1 μM to 1.2 μM (Fig. 5A). Studying the dose-response relationship at Sph concentrations below and above the CMC (Fig. 5B), monomeric Sph had no remarkable effect, in contrast, associated Sph decreased enzyme activity significantly. Similar inhibition values were observed for the dihydro, and dimethyl

lipid derivatives as well. The inhibition by Sph was dependent on the CaM concentration as well: in the presence of 100 μM Sph approx. 10, 25, and 30% remaining activity was measured at 0.1 and 0.6, and 1.2 μM CaM concentrations, respectively. These results indicate that Sph and its analogues in the associated lipid form could inhibit the CaM-dependent NOS activity effectively.

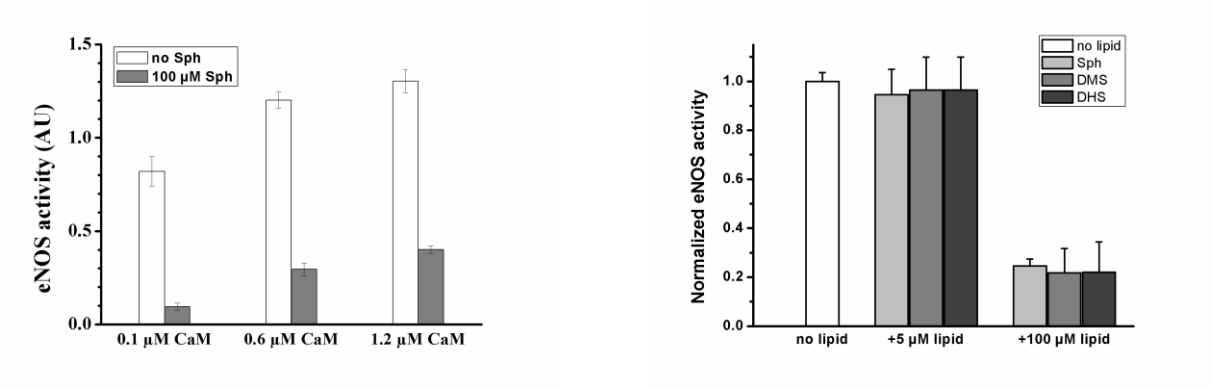


**Figure 5. Effect of Sph and its analogues on the eNOS-acivating ability of CaM**

eNOS activity was measured spectrometrically as described in the Methods section.. (**A**) eNOS activity at various CaM concentrations in the absence and the presence of 100 μM Sph. (**B**) eNOS activity at various Sph concentrations at 0.6 μM CaM. The activity values were normalized to the mean value obtained without the lipid.

MLCK acts as a vasocontractor by catalyzing the phosphorylation of the myosin light chain in the smooth muscle cells *in vivo*. For testing MLCK activity *in vitro*, we have successfully applied the method detecting ADP formed during the kinase reaction *via* first depleting the remaining ATP then converting ADP to ATP by luciferase action, finally detecting the resulting luminescent product, the amount of which is proportional to the ADP from the MLCK reaction. Measuring the CaM-dependence of the CaM-induced activity yielded an $EC_{50}$ value of 7 nM in the absence of Sph (Fig. 6A). The maximal activity was reached at about 100 nM CaM, which concentration was chosen for the lipid dose-response experiments. At a Sph concentration as low as 25 μM, a remarkable rightward shift of the CaM-dependence curve was detected yielding an $EC_{50}$ value of ~1.4 μM (Fig. 6A), which is a 200-fold increase compared to the no lipid case, and indicates potent inhibition of CaM by Sph again. Considering a CMC of 15 μM for Sph, and a micelle build up of 100 monomers, 25 μM Sph solution would contain 0.1 μM micelles, which is equal to the 100 nM CaM concentration applied. Thus, the 200-fold increase in $EC_{50}$ is consistent with a Sph-to-CaM stochiometry ratio of 200:1 in the complex, which would correspond to 1-2 CaMs bound to a single Sph micelle. Testing the lipid-dependence of the MLCK reaction, Sph and its analogues resulted in similar curves with inhibitory concentrations in the 10 μM range (Fig. 6B), at about their CMC values (Fig. 1).

Summarized, it can be concluded that associated Sph might represent a potent inhibitor of CaM function *in vitro*.

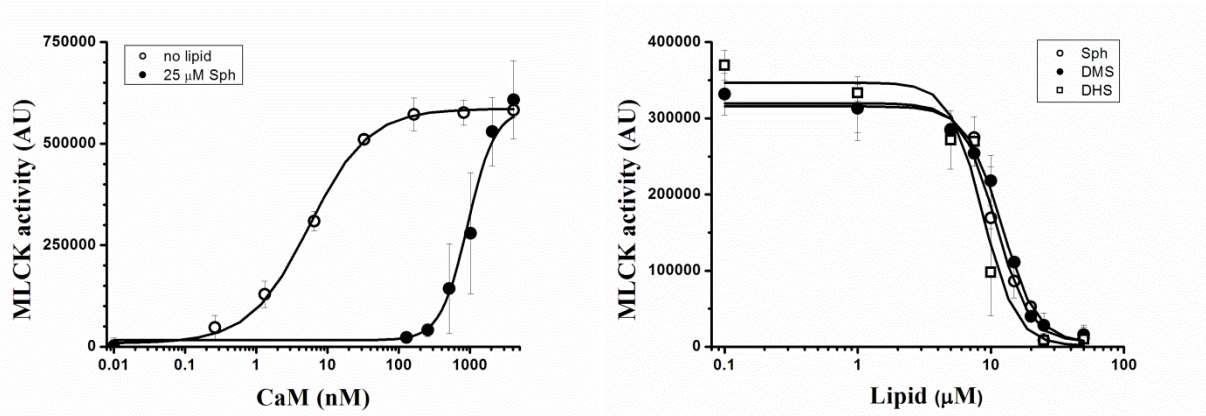


**Figure 6. Effect of Sph on the MLCK-acivating ability of CaM**

MLCK activity was measured detecting the ADP formed in the kinase reaction using the ADP-Glow Kinase Assay kit. Points represent luminescence values subtracted by those measured in the absence of CaM. (**A**) CaM-dependence of the $Ca^{2+}$/CaM -dependent MLCK activity in the absence and the presence of 25 μM Sph. Data were fitted to dose-response curves yielding an $EC_{50}$ of 5.4 ± 0.5 nM, and of 930 ± 134 nM in the absence and the presence of 25 μM Sph, respectively. (**B**) MLCK activity at various Sph, diH-Sph, and DMS concentrations at 100 nM CaM. Similar $IC_{50}$ values of ~ 10 μM and Hill-coefficients of ~3.5 were estimated for the Sph-analogues.

**Effect of sphingosine on NO-mediated vasorelaxation of mouse thoracic aorta**

To test the ability of sphingosine to alter eNOS activity in an intact vessel, myography experiments on mouse thoracic aorta segments were performed. In a previous study we demonstared that acetylcholine (ACh)-induced relaxation is abolished in thoracic aorta prepared from eNOS deficient mice indicating that eNOS mediated this effect [19]. Therefore, ACh dose-responses were compared before and during incubation of the vessels with two different doses of Sph, or their vehicles. Treatment of the vessels with 10 μM Sph for 20 minutes induced a significant rightward shift of the ACh dose-response curve, increasing $EC_{50}$ from 20.4 nM to 73.7 nM (Fig. 1B, n=16). Sphingosine also showed a tendency to decrease $E_{max}$ (from 85.7±2.4 % to 73.9±4.0 %), but this effect was not significant. Increasing the concentration of Sph to 50 μM evoked a robust inhibition of the ACh-mediated relaxation: $EC_{50}$ increased from 21.4 nM to 367 nM, while the maximal relaxing effect decreased from 85.9±2.9 % to 58.3±4.3 % (Fig. 7D, n=16). Incubation of the vessels with the appropriate concentration of vehicle (0.05 or 0.25 % ethanol) resulted in no significant effect (Figures 7A and 1C, n=9 and 16, respectively). In order to decide whether the inhibitory effect of Sph was not due to decreased NO sensitivity of the vascular smooth muscle, SNP-mediated vasorelaxations after treatment with 10 or 50 μM sphingosine, or their vehicles were compared. No significant difference was found between the fitted curves of SNP relaxation after treatment with 0.05 % ethanol, 0.25 % ethanol or 10 μM Sph (Fig. 2, n=3-9). However, incubation with 50 μM Sph resulted in a slight, but significant rightward shift of the dose-response curve compared to its vehicle, with $EC_{50}$ increasing from 14.8 to 36.2 nM (n=9).

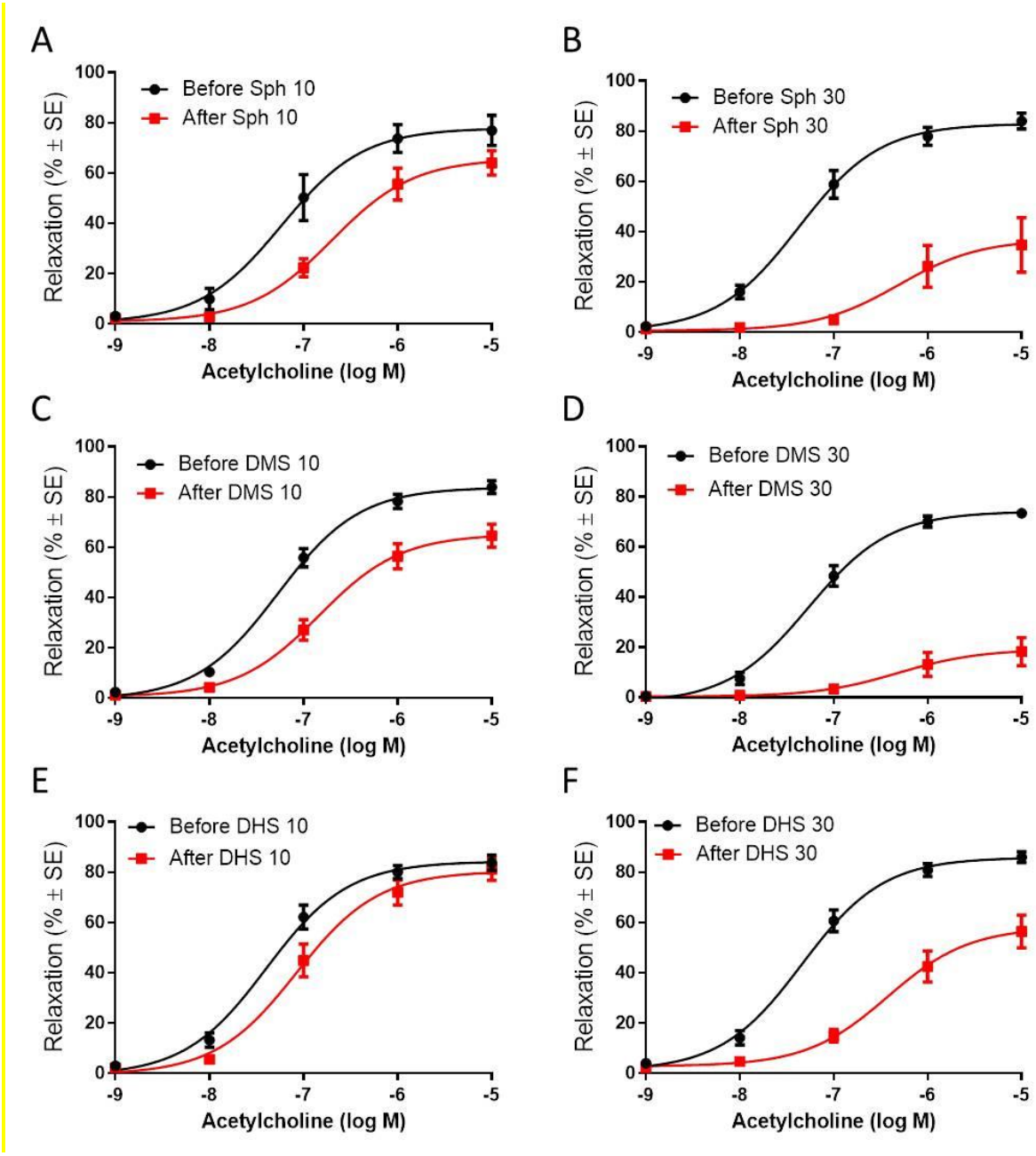


**Figure 7. Effect of sphingolipids on NO-mediated vasorelaxation of mouse thoracic aorta**

ACh dose-response curves upon treatment of the vessels with 10 and 30 μM Sph (**B, D** and **E**), or their vehicles **(A**, **C,** and **E**). The relaxing effect was measured before and during the incubation of the vessels utilizing myography on mouse thoracic aorta. Relaxation values (mean±SE, n=9-16) are expressed as percentage of the precontraction induced by PE.

## Discussion

Recently we have demonstrated that the lipid mediator SPC could inhibit CaM action *in vitro* *via* binding to CaM directly. We hypothesized that the structurally related lipid Sph could exert similar effects, therefore, we explored Sph binding to CaM, and the biological relevance of their interaction focusing on its vascular effects. Besides the simplest sphingolipid Sph, its dihydro, and dimethyl analogues, frequentelly used in …assays as … inhibitors were also studied.

Our findings obtained from *in vitro* binding assays revealed a dynamic complex formation dependent on the lipid association state as well as the $Ca^{2+}$-saturated state of the protein. Fluorescence-based experiments with dansyl-labelled CaM pointed to the ability of CaM to accommodate small lipid clusters of several monomers in the closed protein form, and also to interact with micellar Sph associates, where the protein can modify the integrity of the micelles. The interaction was verified by ITC, which technique highlighted the preferred affinity of CaM to the aggregated lipid state, too.

Thermodynamic parameters of the CaM-Sph interaction determined by ITC showed similarities to SPC binding in several ways regarding the stoichiometry of the two observed binding processes reflecting CaM binding to micelles at lower protein-to-lipid ratios, and micelle disintegration at higher ratios. However, differences in the driving force of the interaction with the two lipids were also revealed. In contrast to the SPC binding, Sph binding was shown to be rather entropically driven.

The crystal structure of $Ca^{2+}$CaM-Sph complex demonstrated directly that $Ca^{2+}$CaM can interact with Sph monomers as also detected by fluorescence spectroscopy and suggested by the stoichiometry of the second binding process in the ITC titration. This binding mode might dominate at higher protein to lipid ratios, or in the presence of lipid monomers rather than Sph patches in membrane environment. Comparing the crystal structures of $Ca^{2+}$CaM-Sph and $Ca^{2+}$CaM-SPC complexes, they share the binding mode of the lipids involving a few (four) monomer chains bound within the central channel of the protein with long regions of the lipid molecules outside the channel being disordered or flexible. Nevertheless, this binding mode with lipids occupying the target peptide site is consistent with a regulation of CaM function of a competitive way.

The different behavior of the two structurally related sphingolipids in the binding assays could mainly be originated in/from the different nature of the lipid head groups. Sph bears a smaller head group with a single positively charged amino-group, whilst the head group of SPC, although bearing a net +1 positive charge as Sph, contains three charged parts: two positively charged ones, and a negatively charged one in between, according to the amino (+), phosphate (-), and choline (+) moieties, respectively. This +-+ charge distribution renders the surface of a SPC micelle remarkably different from that of Sph, which can be manifested in altered binding properties, as detected by ITC. Different headgroup properties can also account for modifications in lipid aggregation processes, where the bigger and less polarized SPC headgroups can contact each other less/more, so that the micelles formed are less/more…. Similarly, the small Sph headgroup could explain the lack of its ordered binding to the negatively charged patches of CaM in the crystal complex.

The biological relevance of the CaM-Sph interaction was tested in i*n vitro* functional assays using several CaM-dependent enzymes. Inhibition of the CaM-dependent activity by Sph for CaN, PDE, eNOS, and MLCK was demonstrated. In the case of CaN and PDE, inhibition of the basal enzyme activity by Sph was also observed to some extent. This can be attributed to some remaining CaM content of the enzyme preparations, or, for CaN, to the CaM-like protein domain. CaM regulates a great number of proteins, besides many enzymes, several ion pumps, ion channels as well. The typical CaM-binding motif is represented by the 25-mer peptide melittin, the binding of which was investigated in a competitive assay utilizing dCaM or melittin fluorescence. The results of the titration of the $Ca^{2+}$CaM-melittin complex are in agreement with the displacement of melittin from CaM. These findings suggest a potent CaM-antagonist role for Sph.

Membrane constituting lipids are widely explored incorporated into model membranes resembling natural membranes, and membrane-born lysophospholipids can be studied in similar ways. However, Sph is known for its ability to move easily between the membrane leaflets, or between membrane and solution, when not stabilizied by certain interactions within the membrane. This, in turn, would result in Sph dissociating the vesicles during measurements, thus, experiments with liposomes were not performed. Instead, *ex vivo* data were collected to explore regulation of CaM activity by Sph in an environment resembling *in vivo* conditions more closely.

Focus was set on the reported vasoactive properties of Sph and their analogues. In line with our *in vitro* findings supporting the ability of Sph to inhibit enzymes eNOS and MLCK involved in the regulation of the vascular tone, the effect of the sphingolipids Sph, DHS, and DMS on the acetylcholine-induced eNOS-mediated relaxation of intact mouse aorta vessels was investigated. Treatment of the vessels with the lipids induced significant rightward shift of the acetylcholine dose-response curve, while a tendency to decrease the maximal relaxing effect upon lipid addition was also observed (Fig. 7). Importantly, no significant effect of Sph and its analogues on the direct NO-donor SNP-mediated vasorelaxation could be detected (Fig Sx), which indicated that the inhibitory effect of Sph is not due to the decreased NO sensitivity of the vascular smooth muscle. NO under physiologic conditions is a vasorelaxant and attenuates inflammation, while its increased production leads to the initiation and progression of inflammation. Our results support the idea that the vascular effects of the sphingolipids used could be due to their influence on the activity of $Ca^{2+}$-calmodulin-dependent eNOS enzyme *via* their binding to calmodulin thereby preventing eNOS activation.

Although vasoactive properties were reported for many sphingolipids, most studies focused on S1P and ceramides. The receptor-mediated action of S1P is well-established, however, the signal transduction mechanism of ceramides, and related sphingolipids is not fully cleared yet. Moreover, controversial effects were reported in several cases. Sph, SPC and S1P were demonstrated to act as vasoconstrictor on isolated microvessels in a concentration-dependent manner [15], with effectiveness in the low micromolar range. Among the sphingolipids tested, SPC showed the highest efficacy over the intermediate effects of Sph and S1P. The authors suggested receptor-mediated mechanism for the action of SPC and S1P-induced vasoconstiction on smooth muscle cells with no significant attenuation of the effect by the release of vasodilatating molecules as NO by the endothelium [15]. In another study, the endothelium-dependent and independent responses after Sph treatment was studied [14].

Similarly to the findings on microvessels above, addition of Sph at 10 μM to precontracted endothelium-intact coronary rings resulted in initial contraction, which was though followed by a slowly developing relaxation, and both processes were shown to be endothelium-dependent. The initial contraction could be abolished by cyclooxigenase inhibitors, while the relaxation was significantly inhibited by the NOS inhibitor L-NMMA. The authors supposed a CaM-dependent relaxation mechanism for the effect of Sph, which is in good agreement with the findings presented here.

Moreover, the fact that sphingolipids can easily be converted to each other makes elucidation of the *in vivo* functional effects of these lipids difficult, and can make interpretation contraversely. itt a nagy kérdés az, hogy az inkubáció alatt a hozzáadott Sph-ból mennyi marad Sph, és mennyi alakul át esetleg vmi más aktív anyaggá. lásd a cikk a jelölt Sph-val [20], mely szerint 5 perc alatt mindenhová eljut egy izolált(?) sejtben, sőt megjelenik ceramidokban (az S1P út blokkolásával). továbbá ehhez: mi van abban a cikkben, ahol 120 percig inkubáltak Sph-val, mert először konstikciót okozott, csak azután relaxált [14]. Nevertheless, our *in vitro* experiments where lipid conversion is not allowed clearly demonstrated the inhibitory potency of all sphingolipids studied. Moreover, we present here direct evidence for the supposed mechanism.

Direct binding of sphingolipids to calmodulin has already been suggested. Some groups of the gangliosides were reported to bind to CaM directly [21], and ganglioside-mediated inhibition of the CaM-dependent enzyme PDE was also argued [22]. Nevertheless, these glycosphingolipids are mostly localized in the outer leaflet of the plasma membrane, and poorly represented in the inner leaflet or the cytosol, thus direct contact with the cytosolic protein CaM is unlikely. In contrast, Sph is formed in the inner leaflet of the plasma-lemma and distributed mainly inside the cell, where it can easily interact with CaM. Summarized, Sph and related sphingolipids like DHS, DMS, and SPC might represent a novel, potent CaM-antagonist class among the lipid mediators.

## Materials and methods

**Preparation of CaM and lipid solutions.** Human recombinant CaM was expressed in *E. coli* and purified using phenyl-sepharose affinity chromatography as described previously [23,24]. Protein purity was checked by SDS-PAGE, and CaM concentration was determined by absorbance using a molar absorption coefficient of 2930 $M^{-1}cm^{-1}$ at 280 nm, or circular dichroism spectroscopy using a molar residual ellipticity of 192,400 deg $cm^2$ at 222 nm in the presence of 1 mM $CaCl_2$ [25]. Dansyl-CaM was prepared according to Kovacs *et al.* [6]
Lipids for the *in vitro* binding assays were purchased from Avanti Polar Lipids (Alabastar, Alabama, USA): Sph (D-erythro-sphingosine, 860490), DMS (N,N-Dimethyl-D-erythro-sphingosine, 860495C, 5 mg/ml in chloroform), and from Sigma: DHS (DL-dihydrosphinganine, approx. 70% erythro, and 28% threo content, D-6783). 10 mM stock solutions were prepared in methanol. Before each experiment, lipid solution were prepared by drying the necessary lipids into glass vials, and resuspending in the appropriate assay buffer, mostly in standard assay buffer (10 mM HEPES, 100 mM KCl, pH 7.2) by vigorous sonication and vortexing. For the *ex vivo* experiments, Sph was purchased from the Cayman Chemical Company (Ann Arbor, MI, USA), and was dissolved in ethanol to get a stock solution of 20 mM.

**Fluorescence spectroscopy.** Spectra were collected using a Jobin Yvon Fluoromax-3 spectrofluorimeter at 25°C in standard assay buffer containing either 1 mM EGTA or $CaCl_2$. Spectra were recorded three times, averaged, and corrected by subtracting the blank (lipid containing buffer). The maximum intensities were read and fitted when measuring dose-dependence curves.
For the dansyl-labeled CaM, the fluorophore was excited at 340 nm, emission was monitored from 400 to 600 nm. Protein and lipid concentrations were 0.2 μM and 100 μM, respectively, or when measuring the dose-dependence for Sph, the lipid concentration varied between 0 and 200 μM.
The CMC (critical micelle concentration) were measured fluorometrically by monitoring the incorporation of 8-anilinonaphtalene-1-sulfonic acid (ANS, Fluka, 10417) [26]. 5 μM ANS was excited in standard assay buffer in the presence of various amounts of lipid at 388 nm, emission was monitored from 410 to 600 nm.
For the melittin binding assay, melittin from honey bee venom got synthesized by EZBiolab (Carmel, IN, USA). Experiments with dansyl-labeled CaM were performed in the presence of 1 mM $CaCl_2$ as described above. Dansyl-CaM, melittin, and lipid concentrations were 0.2, 0.4 μM, and 100 μM, respectively. Trp fluorescence of melittin was measured by excitation at 295 nm using melittin, CaM, and lipid concentrations of 0.6, 1.2, and 100 μM, respectively.

**Isothermal titration calorimetry.** Thermodynamic parameters of the interaction of $Ca^{2+}$CaM and apoCaM with Sph was examined using a VP-ITC or a VP-$ITC_{200}$ instrument (MicroCal, MA). Measurements were performed at 25°C in the standard assay buffer containing either 5 mM $CaCl_2$ or 100 μM EGTA. Aliquots of the protein (45-300 μM) were injected into the ITC

cell containing 200 μM lipid in the same buffer. Titration curves were analyzed and the binding energetics was characterized using the Origin software provided by MicroCal.

**X-ray crystallography.** Details of X-ray diffraction data collection and structure determination are described in Table x.

**NOS activity assay.** Endothelial nitric oxide synthase (eNOS, NOS III, Type III NOS) was purchased from Sigma (N 1533) and enzyme activity was measured using the Ultrasensitive Colorimetric NOS Assay kit and the NOS cofactor mix (Oxford Biomedical Research, NB 78 and NS 70) according the manufacturer's instructions, except that the reaction buffer was 50 mM HEPES, pH 7.4 supplemented with 1 mM $CaCl_2$. Briefly, NO formed by NOS degrades to nitrate and nitrite, nitrate is converted by nitrate reductase to nitrite, and finally nitrite is detected photometrically at 540 nm after treatment with Griess Reagent using a Perkin Elmer EnSpire microplate reader. The 260 μl reaction mixture contained 0.5U eNOS, 0.1, 0.5, or 1.0 μM CaM (0.1 μM added with the NOS cofactor mix, and 0.4 or 0.9 μM CaM was extra added) and 0, 5, or 100 μM Sph. Appropriate blank values of the mixtures lacking NOS were subtracted.

**MLCK activity assay.** Myosin light chain kinase (MLCK) was purchased from Sigma (M9197). Enzyme activity was measured in standard buffer complemented with 0.5 mM $CaCl_2$ and 2.5 mM $MgCl_2$, and 0.1 mg/ml BSA. 20 μl reaction mixtures containing 3.5 ng/μl MLCK, 50 μM ATP, 0.1 mg/ml MLCK substrate (Sigma SCP0196), 0.5 mM DTT, and *i*) 100 nM CaM and various amounts (0-100 μM) of lipids for testing the inhibition by the lipids, or *ii*) 25 μM Sph and various amounts of CaM when measuring the dose-response curves for the CaN activation by CaM. Samples were incubated for 30 minutes at room temperature then the ADP formed during the kinase reaction was detected using the ADP-Glow Kinase Assay kit (Promega) according to manufacturer's instructions.

**Preparation of vessels.** Vessels have been prepared from adult male C57BL/6J mice purchased from Charles River Laboratories (Isaszeg, Hungary). Heparinized (10 IU/ml) Krebs solution (10 ml) was used for transcardial perfusion under deep ether anesthesia as described in detail in [19]. The thoracic aorta was isolated, cleaned of fat and connective tissue under a dissection microscope (M3Z, Wild Heerbrugg AG, Gais, Switzerland) and immersed in Krebs solution of the following millimolar composition: NaCl 119, KCl 4.7, $KH_2PO_4$ 1.2, $CaCl_2 \cdot 2H_2O$ 2.5, $MgSO_4 \cdot 7H_2O$ 1.2, $NaHCO_3$ 20, EDTA 0.03, and glucose 10 at room temperature. Three mm long ring segments were prepared and mounted on stainless steel vessel holders (200 μm in diameter) in a conventional myograph setup (610M Multi Wire Myograph System, Danish Myo Technology A/S, Aarhus, Denmark). Special care was taken to preserve the endothelium. The IACUC of the Semmelweis University reviewed and approved all of the procedures.

**Myography.** Organ chambers of the myographs were filled with 6 ml Krebs solution and aerated with carbogen. The vessels were then allowed a 30 min equilibration period.

Meanwhile the bath solution was warmed to 37 ºC and the resting tension was adjusted to 15 mN that was determined to be optimal in a previous study [19]. Thereafter, the vessel segments were exposed to 124 mM $K^+$ Krebs solution (made by isoosmolar replacement of $Na^+$ by $K^+$) for 1 min. Following several washes with normal Krebs solution, during which the vascular tension returned to the resting level, the vessels were contracted by 10 μM phenylephrine (PE) and relaxed by 0.1 μM acetylcholine in order to roughly test the reactivity of the smooth muscle and endothelium, respectively. After repeated washing, the segments were exposed to 124 mM $K^+$ Krebs solution for 3 min in order to elicit reference contraction. Thirty minutes later, cumulative concentrations of PE (10 nM-10 μM) was administered in order to determine the reactivity of the smooth muscle. After a stable plateau, acetylcholine (ACh) – a vasorelaxant primarily acting via endothelial NO release – was applied in cumulative doses (1 nM-10 μM). This was followed by a 30 min resting period. To test the effect of Sph on NO mediated vasorelaxation, PE and ACh dose-response was repeated after 20 min incubation with 10 or 50 μM Sph or their vehicle (0.05 or 0.25 % ethanol, respectively). In another set of experiments, the second ACh dose-response was changed to the NO donor sodium-nitroprusside (SNP, 1 nM-10 μM), in order to test the relaxing ability of smooth muscle to exogenous NO. To reach the final concentration of 10 or 50 μM, 3 or 15 μl of the 20 mM stock solution was added to the organ chambers, respectively. As control, 3 or 15 μl of ethanol were administered, giving a final concentration of 0.05 or 0.25 % in the organ chamber. Drugs and chemicals except the lipids were purchased from Sigma-Aldrich (St. Louis, MO, USA). Changes of the vascular tension were recorded with the MP100 System and analyzed with the AcqKnowledge 3.7.3 software of BIOPAC System Inc. (Goleta, CA, USA). Vasorelaxations were expressed as percent of the precontraction produced by PE.

**Data Analysis and Statistics.** Data analysis was done by GraphPad Prism 6 software (GraphPad Software Inc., La Jolla, CA, USA), or the Origin software (OriginLab Corporation, Northampton, MA, USA). Best-fit values of $EC_{50}$ and maximal responses ($E_{max}$) of the dose-response curves were calculated by nonlinear regression curve fitting, followed by extra sum-of-squares F-test. Changes were considered significant if $p < 0.05$. Data are presented as mean ± standard error of mean (SE) and *N* indicates the number of samples tested.

## Acknowledgements

This work was supported by the Hungarian Scientific Research Fund OTKA (grants K82092 to K.L., PD104344 to T.J. and K112964 to Z.B.). We acknowledge the European Synchrotron Radiation Facility for provision of synchrotron radiation facilities and …. We thank Dr. Ferenc Tölgyesi and the Institute of Biophysics and Radiation Biology, Semmelweis University, Budapest for providing the instrumentation for calorimetry experiments (VP ITC).

## References


1. Chattopadhyaya, R., Meador, W.E., Means, A.R. & Quiocho, F.A. Calmodulin structure refined at 1.7 A resolution. *J Mol Biol* **228**, 1177-92 (1992).
2. LaPorte, D.C., Wierman, B.M. & Storm, D.R. Calcium-induced exposure of a hydrophobic surface on calmodulin. *Biochemistry* **19**, 3814-9 (1980).
3. Meador, W.E., Means, A.R. & Quiocho, F.A. Modulation of calmodulin plasticity in molecular recognition on the basis of x-ray structures. *Science* **262**, 1718-21 (1993).
4. Mata, R. et al. Calmodulin inhibitors from natural sources: an update. *J Nat Prod* **78**, 576-86 (2015).
5. Kovacs, E. et al. Structure and mechanism of calmodulin binding to a signaling sphingolipid reveal new aspects of lipid-protein interactions. *Faseb J* **24**, 3829-39 (2010).
6. Kovacs, E. & Liliom, K. Sphingosylphosphorylcholine as a novel calmodulin inhibitor. *Biochem J* **410**, 427-37 (2008).
7. Kovacs, E., Toth, J., Vertessy, B.G. & Liliom, K. Dissociation of calmodulin-target peptide complexes by the lipid mediator sphingosylphosphorylcholine: implications in calcium signaling. *J Biol Chem* **285**, 1799-808 (2009).
8. Colina, C., Cervino, V. & Benaim, G. Ceramide and sphingosine have an antagonistic effect on the plasma-membrane Ca2+-ATPase from human erythrocytes. *Biochem J* **362**, 247-51 (2002).
9. Jefferson, A.B. & Schulman, H. Sphingosine inhibits calmodulin-dependent enzymes. *J Biol Chem* **263**, 15241-4 (1988).
10. Viani, P., Giussani, P., Riboni, L., Bassi, R. & Tettamanti, G. Sphingosine inhibits nitric oxide synthase from cerebellar granule cells differentiated in vitro. *FEBS Lett* **454**, 321-4 (1999).
11. Cuvillier, O. Sphingosine in apoptosis signaling. *Biochim Biophys Acta* **1585**, 153-62 (2002).
12. Woodcock, J. Sphingosine and ceramide signalling in apoptosis. *IUBMB Life* **58**, 462-6 (2006).
13. Jin, J.S., Tsai, C.S., Si, X. & Webb, R.C. Endothelium dependent and independent relaxations induced by ceramide in vascular smooth muscles. *Chin J Physiol* **42**, 47-51 (1999).
14. Murohara, T. et al. Effects of sphingomyelinase and sphingosine on arterial vasomotor regulation. *J Lipid Res* **37**, 1601-8 (1996).
15. Bischoff, A. et al. Sphingosine-1-phosphate and sphingosylphosphorylcholine constrict renal and mesenteric microvessels in vitro. *Br J Pharmacol* **130**, 1871-7 (2000).
16. Czyborra, P. et al. Transient relaxation of rat mesenteric microvessels by ceramides. *Br J Pharmacol* **135**, 417-26 (2002).
17. Contreras, F.X., Sot, J., Alonso, A. & Goni, F.M. Sphingosine increases the permeability of model and cell membranes. *Biophys J* **90**, 4085-92 (2006).
18. Brokx, R.D., Lopez, M.M., Vogel, H.J. & Makhatadze, G.I. Energetics of target peptide binding by calmodulin reveals different modes of binding. *J Biol Chem* **276**, 14083-91 (2001).
19. Horvath, B., Orsy, P. & Benyo, Z. Endothelial NOS-mediated relaxations of isolated thoracic aorta of the C57BL/6J mouse: a methodological study. *J Cardiovasc Pharmacol* **45**, 225-31 (2005).

20. Haberkant, P. et al. Bifunctional Sphingosine for Cell-Based Analysis of Protein-Sphingolipid Interactions. *ACS Chem Biol* **11**, 222-30 (2016).
21. Higashi, H., Omori, A. & Yamagata, T. Calmodulin, a ganglioside-binding protein. Binding of gangliosides to calmodulin in the presence of calcium. *J Biol Chem* **267**, 9831-8 (1992).
22. Higashi, H. & Yamagata, T. Mechanism for ganglioside-mediated modulation of a calmodulin-dependent enzyme. Modulation of calmodulin-dependent cyclic nucleotide phosphodiesterase activity through binding of gangliosides to calmodulin and the enzyme. *J Biol Chem* **267**, 9839-43 (1992).
23. Gopalakrishna, R. & Anderson, W.B. Ca2+-induced hydrophobic site on calmodulin: application for purification of calmodulin by phenyl-Sepharose affinity chromatography. *Biochem Biophys Res Commun* **104**, 830-6 (1982).
24. Szeltner, Z. et al. GAP43 shows partial co-localisation but no strong physical interaction with prolyl oligopeptidase. *Biochim Biophys Acta* **1804**, 2162-76 (2010).
25. Harmat, V. et al. A new potent calmodulin antagonist with arylalkylamine structure: crystallographic, spectroscopic and functional studies. *J Mol Biol* **297**, 747-55 (2000).
26. Abuin, E.B., Lissi, E.A., Aspee, A., Gonzalez, F.D. & Varas, J.M. Fluorescence of 8-Anilinonaphthalene-1-sulfonate and Properties of Sodium Dodecyl Sulfate Micelles in Water-Urea Mixtures. *J Colloid Interface Sci* **186**, 332-8 (1997).

# Supplementary material

## SPHINGOSINE INHIBITS CALMODULIN ACTION: IMPLICATION FOR REGULATION OF ENDOTHELIAL NITRIC OXIDE SYNTHASE-MEDIATED VASORELAXATION

Tünde Juhász[a], Éva Ruisanchez[b], Veronika Harmat[c,d], József Kardos[e], Mónika Kabai Viktor Erdősi[b] Zoltán Benyó[b], Károly Liliom[f]

[a]Institute of Materials and Environmental Chemistry, Research Centre for Natural Sciences, Hungarian Academy of Sciences, Magyar Tudósok krt. 2, Budapest, H-1117 Hungary

[b] Institute of Human Physiology and Clinical Experimental Research, Semmelweis University, Tűzoltó u. 37–47, H-1094 Budapest, Hungary

[c]Laboratory of Structural Chemistry and Biology, Institute of Chemistry, Eötvös Loránd University, Pázmány Péter sétány 1/A, H-1117 Budapest, Hungary

[c]Protein Modelling Research Group, Hungarian Academy of Sciences - Eötvös Loránd University, Pázmány Péter sétány 1/A, H-1117 Budapest, Hungary

[e]Department of Biochemistry, Eötvös Loránd University, Pázmány Péter sétány 1/C, H-1117 Budapest, Hungary

[f]Department of Biophysics and Radiation Biology, Semmelweis University, Tűzoltó u 37-47, Budapest, H-1094 Hungary,

**Figure S1. Sph binds to CaM in a concentration dependent manner**

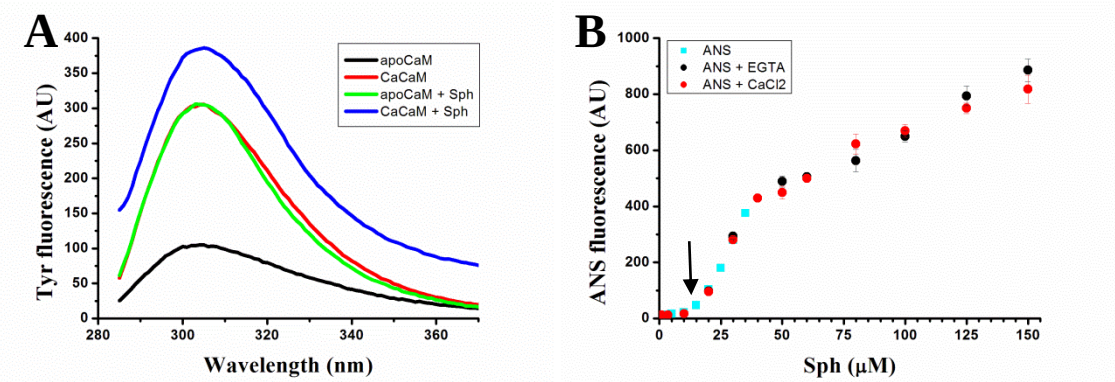


(**A**) Fluorescence spectra of apo- and $Ca^{2+}$-saturated CaM (1.0 μM) in the absence and presence of 100 μM Sph. (**B**) CMC of Sph. Data were measured in the presence of 5 μM ANS, and the CMC was estimated to be ~10 μM (indicated by the arrow).

CaM contains no tryptophan but two tyrosine residues in the C-terminal domain, the fluorescence intensity of which is sensitive to the $Ca^{2+}$-loaded state of the domain. An increase of ~3-fold could be measured upon $Ca^{2+}$-binding, which is in agreement with the reported quenching of the tyrosine fluorescence in apoCaM [1]. In the presence of 100 μM Sph, the spectrum of apoCaM changed to one very similar to that observed for $Ca^{2+}$-saturated CaM without the lipid. For the $Ca^{2+}$CaM, addition of the lipid at 100 μM elevated the fluorescence intensity by further ~30-35 %.

**Figure S2. Crystal structure of the $Ca^{2+}$CaM/Sph complex**

**Figure S3. CaM-melittin interaction in the presence of sphingolipids.**

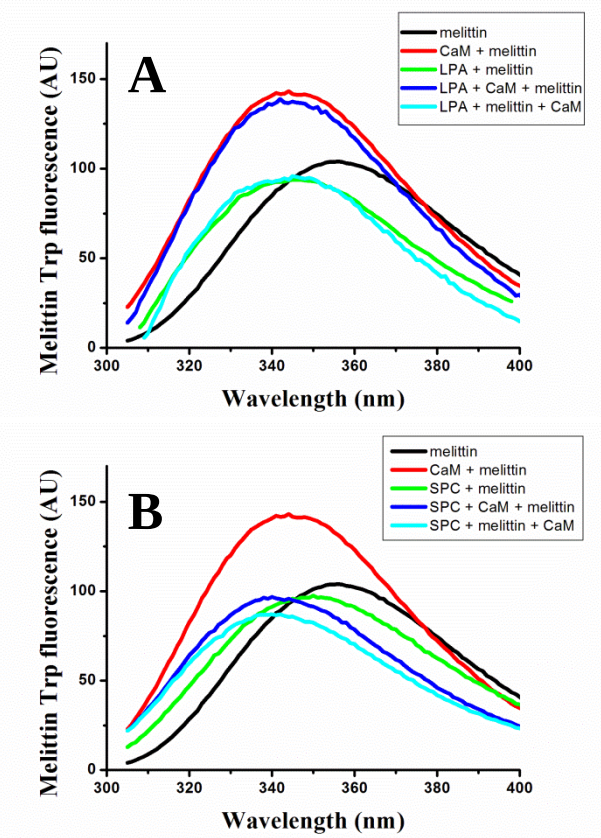


Fluorescence spectra of melittin (0.6 μM) in the absence and presence of CaCaM (1.2 μM), and 100 μM LPA (**A**) or SPC (**B**). In the case of the three-component mixtures, the two listed first were preincubated followed by the addition of the third listed component. The binding events referring to the spectral changes in melittin Trp fluorescence in the presence of CaM and the lipids are summarized in Table S1 (see also Fig. 4 in main text).

**Table S1.** Interactions in the melittin-CaM-sphingolipid three-component systems identified by melittin Trp fluorescence.

| | Sph | LPA | SPC |
|---|---|---|---|
| CaM interacts with the lipid | yes | no | yes |
| Melittin interacts with the lipid | no | yes | yes |
| (Lipid + CaM) + melittin | | | |
| Melittin is | free | bound to CaM | bound to CaM and lipid |
| CaM is | bound to lipid | bound to melittin | bound to melittin and lipid |
| (Lipid + melittin) + CaM | | | |
| Melittin is | free | bound to lipid | bound to CaM and lipid |
| CaM is | bound to lipid | free | bound to melittin and lipid |

**Figure S4. Effect of Sph on the PDE-activating ability of CaM**

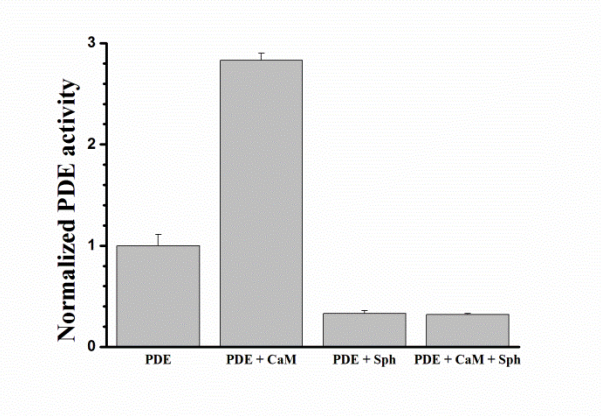


Basal and $Ca^{2+}$/CaM-dependent PDE activity in the absence and the presence of 100 μM Sph. PDE activity was measured fluorimetrically following the consumption of the substrate mant-cGMP. The bars depict the initial rate of the reaction normalized to the basal PDE activity measured in the absence of added $Ca^{2+}$CaM. Data points are mean±SEM, n=3-6.

The effect of Sph on the CaM-dependent activity of PDE was examined. We have found that (i) CaM induced a significant, approximately 3-fold increase in the enzyme activity, (ii) addition of 100 μM Sph decreased the basal PDE activity down to ~ 30-35 %, and (iii) adding CaM and Sph together, the activity observed was very similar to that without CaM. These indicated that Sph at concentrations above its CMC inhibited the activating ability of CaM but also the basal PDE activity. The former observation is consistent with previous findings reporting that Sph inhibits the PDE activity in the presence of CaM [2]. Specifically, a remaining $Ca^{2+}$/CaM-induced activity of ~10% was found in the presence of 100 μM Sph [2], which agrees well with our results of that of ~12 %. We have also shown that the remaining activity arises from the basal activity alone since the addition of CaM could not induce any elevation in the PDE activity. These results indicate that the activating ability of CaM is fully inhibited in the presence of associated Sph.

**Figure S5. Effect of Sph on the CaN-activating ability of CaM**

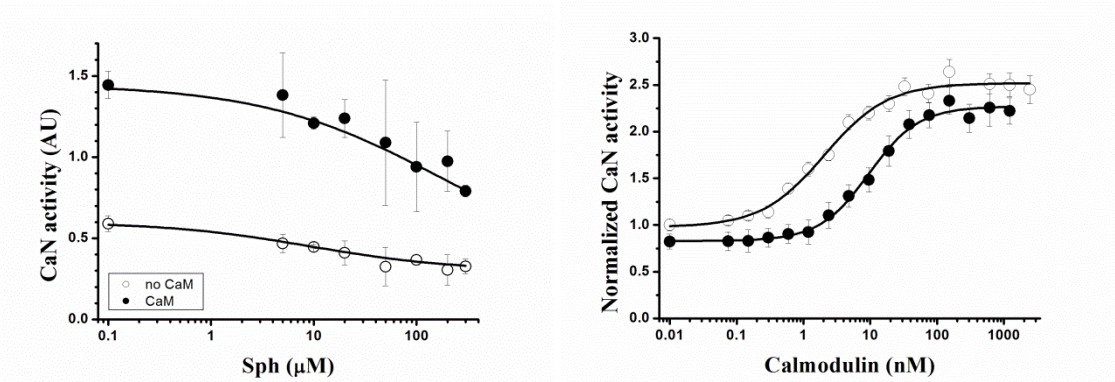


(**A**) Lipid-dependence of the CaN activity in the presence and absence of CaM. Data are relative initial values. To get a reliable fit to the data measured with CaM, the end point (at high Sph concentrations) was set to the value obtained without CaM. Dose-dependence curves estimated an $IC_{50}$ of 20 ± 2 nM, and of 171 ± 18 nM in the absence and the presence of 0.6 μM CaM, respectively. Hill-coefficients were 0.5 ± 0.1 in both cases. (**B**) CaM-dependence of the $Ca^{2+}$/CaM-dependent CaN activity in the absence and the presence of Sph. CaN activity was measured photometrically following the consumption of the substrate PNPP. Points represent the initial rate of the reaction normalized to the basal CaN activity measured in the absence of CaM. Data were fitted to dose-response curves yielding an $EC_{50}$ of 2.1 ± 0.2 nM and of 9.5 ± 0.9 nM in the absence and the presence of 150 μM Sph, respectively.

The effect of Sph on CaM activity was also tested on calcineurin. In the absence of the lipid, we have shown an approximately 2.5-fold elevation in the enzyme activity by CaM with a half-activation concentration of 2.4±0.5 nM (Fig.S5A). Measuring the dose-dependence of the activation by CaM in the presence of Sph, we could detect a slight (~15-20%) decrease in the basal as well as the maximal CaN activity, and a right shift of the curve to higher $EC_{50}$ values compared to that observed without the lipid. The former phenomenon might be explained by the binding of Sph to either the CaM may present in the CaN preparation, or to calcineurin B, the calmodulin-like calcineurin subunit. The latter effect is consistent with the competitive inhibition of the CaM induced activation of CaN by Sph.

The dose-dependence of the effect of Sph was also analyzed, yielding an $IC_{50}$ as high as ~170 μM for the activation by CaM (Fig. S5B), which is one order of magnitude higher than the CMC value for Sph determined in the standard assay buffer. The rather high value and the rather low Hill-coefficient (~0.5 in contrast to the values of 2-3 seen in other measurements or when using SPC) is consistent with the significantly reduced ability for Sph to go into solution under the assay conditions when using our standard preparation procedure for dissolving the lipids (*i.e.* vortex/sonication after drying the lipids with nitrogen to glass tubes). The high amount (20 mM) of phosphates presented by the substrate PNPP might have precluded solvation of the lipid since dilution of Sph from a clear, PNPP-free solution into a PNPP containing one resulted in an opalescent solution that could not fully cleared upon

sonication. This indicates that Sph micelles might form higher aggregates, which in turn results in lowering the lipid surface available for interaction. Using these Sph solutions at nominal concentrations of 150 μM, the CaM-dependence curves yielded apparent $EC_{50}$ values of ~10 nM (Fig. 6A) compared to ~2 nM measured without the lipid. Since Sph is expected to be a potent inhibitor of CaM function above the CMC value in its associated form, the fact that the assay condition might interfere with Sph micelle formation can easily result in rather similar $EC_{50}$ values of the CaM activation curves in the presence and the absence of lipid as observed here.

**Figure S6. SNP mediated vasorelaxation in the presence of sphingolipids.**

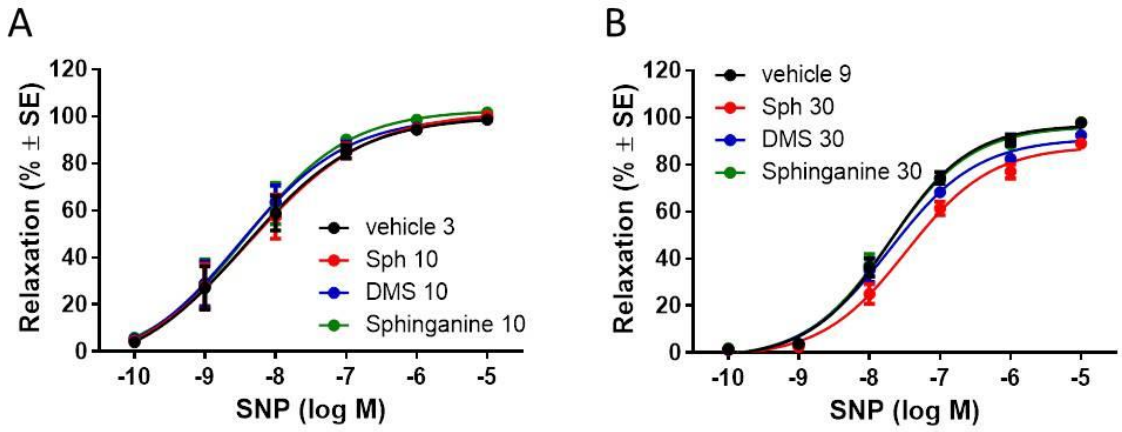


SNP (sodium nitroprusside) dose-response curves upon treatment of the vessels with 10 and 30 μM Sph, or their vehicles. The relaxing effect was measured before and during the incubation of the vessels utilizing myography on mouse thoracic aorta. Relaxation values (mean±SE, n=9-16) are expressed as percentage of the precontraction induced by PE.

## Methods

**Calcineurin activity assay.** Calcineurin (PPase-2B, CaN) was purchased from Promega (V6361). Dephosphorylation of the substrate p-nitrophenyl phosphate (PNPP, Sigma, 1040) was followed by monitoring the increase in absorbance at 405 nm using a Perkin Elmer EnSpire microplate reader. CaN activity was assayed by measuring initial velocities at 28 °C in 50 mM Tris, pH 7.5 containing 0.001 unit/µl CaN, 0.2 mg/ml BSA, 20 mM PNPP, 1 mM $NiCl_2$, and *i*) 10 µg/ml CaM and various amounts of Sph for testing the inhibition by Sph, or *ii*) 150 µM Sph and various amounts of CaM when measuring the dose-response curves for CaN activation by CaM.

**PDE activity assay.** Phosphodiesterase I, 3',5'-cyclic-nucleotide-specific (PDE) from bovine brain was purchased from Sigma (9529) and mant-cGMP from Calbiochem (370668). PDE activity was measured fluorometrically by monitoring the consumption of mant-cGMP as described by Johnson *et al.* [3], so as mant-cGMP was excited at 280 nm and emission was monitored at 450 nm. The reaction was followed at 25 °C in standard assay buffer containing 5 mM $MgCl_2$, and either 1 mM $CaCl_2$ or 1 mM EGTA. Mant-cGMP, PDE, CaM and lipid concentrations were 10 µM, 6.5 nM, 100 nM, and 125 µM, respectively. The initial velocities of the substrate hydrolysis were measured in the absence and in the presence of CaM, yielding the basal and the CaM-dependent activities, respectively.

## References:


1. VanScyoc, W.S. et al. Calcium binding to calmodulin mutants monitored by domain-specific intrinsic phenylalanine and tyrosine fluorescence. *Biophys J* **83**, 2767-80 (2002).
2. Jefferson, A.B. & Schulman, H. Sphingosine inhibits calmodulin-dependent enzymes. *J Biol Chem* **263**, 15241-4 (1988).
3. Johnson, J.D., Walters, J.D. & Mills, J.S. A continuous fluorescence assay for cyclic nucleotide phosphodiesterase hydrolysis of cyclic GMP. *Anal Biochem* **162**, 291-5 (1987).

# ENHANCED ENDOTHELIAL NITRIC OXIDE SYNTHASE MEDIATED VASORELAXATION BY SPHINGOMYELINASE IN DB/DB MICE

Éva Ruisanchez[a,*], Rita Cecília Panta[a,*], Levente Kiss[b,*], Zsuzsa Straky[a], Dávid Korda[a], Adrienn Párkányi[a], Károly Liliom[c], Gábor Tigyi[d], Zoltán Benyó[a]

[a]*Institute of Translational Medicine,* [b]*Department of Physiology, and* [c]*Institute of Biophysics and Radiation Biology, Semmelweis University, 37-47 Tűzoltó street, H-1094, Budapest, Hungary*

[d]*Department of Physiology, University of Tennessee, Health Science Center, 3 Dunlap Avenue Rm C326, Memphis, TN 38163, USA*

**These authors contributed equally to the work*

ruisanchez.eva@med.semmelweis-univ.hu
sokszem@gmail.com
kiss.levente@med.semmelweis-univ.hu
straky.zsuzsa@gmail.com
kordadavid@t-online.hu
padrisz@gmail.com
liliom.karoly@med.semmelweis-univ.hu
gtigyi@uthsc.edu
benyo.zoltan@med.semmelweis-univ.hu

**Corresponding author: Zoltán Benyó, MD, PhD, DSc**
*benyo.zoltan@med.semmelweis-univ.hu*
*Institute of Translational Medicine, Semmelweis University*
*POB 2, H-1428 Budapest, Hungary*

**Abstract**

Sphingolipids are important biological mediators both in health and in metabolic diseases. We aimed to investigate the vascular effects of enhanced sphingomyelinase (SMase) activity in a mouse model of type 2 diabetes mellitus (T2DM) and to gain understanding of the secondary signaling pathways involved. In phenylephrine precontracted aortic segments of non-diabetic mice 0.2 U/ml neutral SMase induced transient contraction and subsequent weak relaxation, whereas vessels of db/db mice showed marked relaxation. In the presence of the thromboxane prostanoid receptor (TP) antagonist SQ 29,548, SMase induced enhanced relaxation in both groups, which was 3-fold stronger in vessels of db/db mice as compared to controls. Co-administration of the nitric oxide synthase (NOS) inhibitor L-NAME abolished the vasorelaxation in both groups. Our results indicate dual vasoactive effects of SMase: TP-mediated vasoconstriction and NO-mediated vasorelaxation. Surprisingly, in spite of the general endothelial dysfunction in T2DM, the endothelial NOS-mediated vasorelaxant effect of SMase is markedly enhanced.

**Keywords**

Sphingolipids, sphingomyelinase, vasorelaxation, endothelial nitric oxide synthase, type 2 diabetes, thromboxane prostanoid receptor

**Abbreviations**

*ACh – Acetylcholine*
*C1P – Ceramide-1-phosphate*
*NOS – Nitric oxide synthase*
*PE – Phenylephrine*
*S1P – Sphingosine-1-phosphate*
*SM – Sphingomyelin*
*SMase – Sphingomyelinase*
*Sph – Sphingosine*
*T2DM – Type 2 diabetes mellitus*
*TP – Thromboxane prostanoid receptor*

**Graphical abstract**

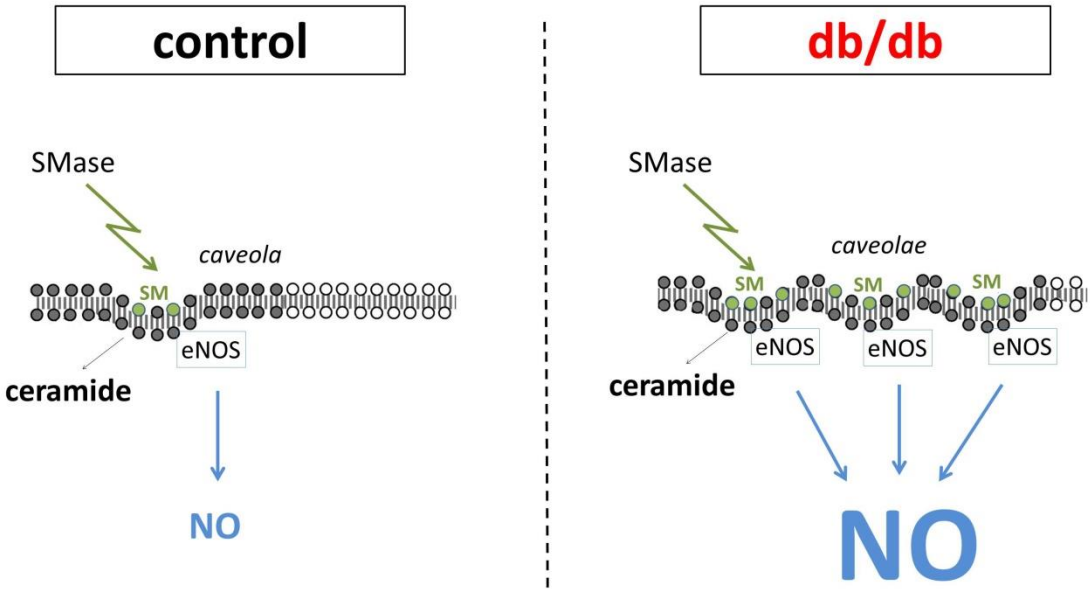


**Highlights**

Sphingomyelinase induces biphasic vascular tension changes in health and in diabetes

The transient vasocontraction is mediated by thromboxane prostanoid (TP) receptors

The subsequent eNOS-mediated vasorelaxation is enhanced paradoxically in diabetes

## 1. Introduction

Sphingolipids, derived from sphingomyelin metabolism, have been implicated as important mediators in the physiology and pathophysiology of the cardiovascular system [1-6]. Sphingomyelinase (SMase) catalyzes the conversion of sphingomyelin to ceramide, which is the precursor of other sphingolipid mediators including ceramide-1-phosphate (C1P), sphingosine (Sph) and sphingosine-1-phosphate (S1P) [7]. The majority of S1P-induced biological effects are mediated by G-protein-coupled receptors (GPCR), termed $S1P_{1-5}$ [8]. Other sphingolipid mediators may have biological effects independently of the activation of S1P receptors by directly interacting with membrane or intracellular protein targets [5, 9-11].

Based on the optimal pH for their catalytic activity, SMase isoforms can be divided into three groups: alkaline, acidic and neutral [12]. Whereas the expression and known functions of alkaline SMase are mostly restricted to the gastrointestinal system, acidic and neutral SMases are more widely expressed and involved in physiological and pathophysiological reactions of many organs including the cardiovascular system. In the vasculature SMases are implicated in the regulation of vascular tone and permeability as well as causing atherosclerotic lesions and vascular wall remodeling [13]. Interestingly, neutral SMase has been reported to induce a wide range of changes in the vascular tone, depending on the species, vessel type and experimental conditions (Table 1.). Taken into account the large number of biologically active mediators (including ceramides, ceramide-1-phosphate, sphingosine and sphingosine-1-phosphate) that can be generated both extra- and intracellularly upon triggering the sphingolipid biosynthesis by neutral SMase the diversity of vascular effects is not unexpected.

SMase enzymes are reportedly upregulated in certain cardiovascular and metabolic disorders such as type 2 diabetes mellitus (T2DM) [13-15]. Sphingolipids have been implicated as important regulators of inflammatory processes in diabetes [16]. Stress conditions initiate changes in sphingolipid metabolism [17], and sphingolipids have emerged as key mediators of stress responses [18, 19]. Extracellular stressors induce sphingolipid synthesis and turnover, thereby ‘remodeling’ sphingolipid profiles and their topological distribution within cells [20]. Emerging evidence not only demonstrates profound changes in sphingolipid pools and distribution under conditions of overnutrition

[21-23], but also implicates sphingolipids in mediating cell-signaling responses that precipitate pathology associated with obesity [24]. In spite of the marked alterations in the metabolism and actions of sphingolipids in diabetes and recent observations indicating that ceramide may contribute to the development of diabetic endothelial dysfunction [25], relatively little is known about the effects of sphingolipids on vascular functions in T2DM. In the present study, we aimed to analyze the effects of SMase on vascular tone under diabetic conditions and to elucidate the signaling mechanisms involved.

| Species | Vessel | Vasoactive effects | Proposed mechanism | Reference |
|---|---|---|---|---|
| Yorkshire pig | coronary artery | transient endothelium-dependent contraction followed by endothelium-dependent relaxation | vasoconstriction: prostanoid(s)<br>vasorelaxation: NO | [26] |
| Sprague-Dawley rat | thoracic aorta | endothelium-independent relaxation | inhibition of PKC | [27, 28] |
| Wistar rat | thoracic aorta | partly endothelium-independent relaxation | endothelium-mediated component is independent of NO or prostanoids<br>non-endothelial component is independent of PKC | [29] |
| Mongrel dog | basilar artery | endothelium-independent contraction | activation of VDCC and PKC | [30] |
| Wistar rat | pial venule (60-70 μm in diameter) | constriction and spasm | activation of VDCC, PKC and MAP kinase | [31] |
| Wistar rat | thoracic aorta | endothelium-independent relaxation | inhibition of both $Ca^{2+}$-dependent and -independent (RhoA/Rho-kinase mediated) contractile pathways | [32] |
| Cow | coronary artery | endothelium-dependent relaxation | $Ca^{2+}$-independent eNOS activation, involving phosphorylation on serine 1179 and dissociation of eNOS from plasma membrane caveolae | [33] |
| Wistar rat | pulmonary artery | endothelium-independent contraction | activation of VDCC, PKCζ and Rho-kinase | [34] |
| Wistar-Kyoto (WKY) and spontaneously hypertensive rat (SHR) | carotid artery | SHR: strong endothelium-dependent contraction<br>WKY: weak endothelium-dependent contraction | vasoconstriction is mediated by $PLA_2$- and COX2-mediated $TXA_2$ release and attenuated by NO | [35-37] |

**Table 1. Reported vasoactive effects of neutral SMase**

## 2. Materials and Methods

All procedures were carried out according to the guidelines of the Hungarian Law of Animal Protection (28/1998) and were approved by the National Scientific Ethical Committee on Animal Experimentation (PEI/001/2706-13/2014).

### *2.1. Animals and general procedures*

The BKS db diabetic mouse strain was obtained from The Jackson Laboratory (Bar Harbor, ME, USA) and has been maintained in our animal facility by mating repulsion double heterozygotes (Dock7$^{m}$/+, +/Lepr$^{db}$). Littermate adult male diabetic (Lepr$^{db}$/Lepr$^{db}$ referred as db/db) and misty (Dock$^{7m}$/Dock$^{7m}$ referred as control) mice were selected for experiments. Animals were weighted and blood samples were collected by cardiac puncture followed by transcardial perfusion with 10 mL heparinized (10 IU/mL) Krebs solution under deep ether anesthesia as described previously [38]. Nonfasting blood glucose was measured by Dcont IDEÁL biosensor type blood glucose meter (77 Elektronika Kft., Budapest, Hungary). In some experiments, additional blood samples were collected, allowed to clot for 30 min at room temperature, centrifuged at 2000 x g for 15 min at 4 °C and serum was snap frozen for later phosphorylcholine assay, which was based on the method described by Hojjati and Jiang [39] using a commercially available kit (Item № 10009928, Cayman Chemical, Ann Arbor, MI, US).

### *2.2. Myography*

The thoracic aorta was removed and cleaned of fat and connective tissue under a dissection microscope (M3Z, Wild Heerbrugg AG; Gais, Switzerland) and immersed in a Krebs solution of the following composition (mmol/L): 119 NaCl, 4.7 KCl, 1.2 $KH_2PO_4$, 2.5 $CaCl_2 \cdot 2H_2O$, 1.2 $MgSO_4 \cdot 7H_2O$, 20 $NaHCO_3$, 0.03 EDTA, and 10 glucose at room temperature and pH 7.4. Vessels were cut into ~3 mm-long segments and mounted on stainless steel vessel holders (200 µm in diameter) in a conventional myograph setup (610 M multiwire myograph system; Danish Myo Technology A/S; Aarhus, Denmark). Special care was taken to preserve the endothelium.

Wells of the myographs were filled with 8 mL Krebs solution aerated with carbogen. The vessels were allowed a 30-min resting period, during which the bath solution was warmed up to 37 $^{o}$C and the passive tension was adjusted to 15 mN, which was determined to be optimal in a previous study [38]. Subsequently, the tissues were exposed to 124 mmol/L $K^+$ Krebs solution (made by isomolar replacement of $Na^+$ by $K^+$) for 1 min, followed by several washes with normal Krebs solution. A contraction evoked by 10 µmol/L phenylephrine (PE) followed by administration of 0.1 µmol/L acetylcholine (ACh) served as a test of the reactivity of the smooth muscle and the endothelium, respectively. After repeated washing, during which the vascular tension returned to the resting level, the segments were exposed to 124 mmol/L $K^+$ Krebs solution for 3 min in order to elicit a reference maximal contraction. Subsequently, after a 30-min washout, increasing concentrations of PE (0.1 nmol/L to 10 µmol/L) and ACh (1 nmol/L to 10 µmol/L) were administered to determine the reactivity of the smooth muscle and the endothelium, respectively. Following a 30-min resting period, the vessels were precontracted to 70-90% of the reference contraction by an appropriate concentration of PE and after contraction has stabilized, the effects of 0.2 U/ml nSMase (Sphingomyelinase from B. cereus, Sigma-Aldrich, St. Louis, MO, USA) were investigated for 20 min. Bacterial sphingomyelinase functions in neutral pH, and is reportedly a useful tool to mimic the biological effects of activation of cellular SMase [40, 41]. In some experiments, selective thromboxane prostanoid receptor (TP) antagonist SQ-29548 (1 µM) with or without the NOS inhibitor L-NAME (100 µM) was applied to the baths 30 min prior to administration of nSMase. Finally, to test the sensitivity of the smooth muscle to NO, sodium nitroprusside (SNP, 0.1 nmol/L to 10 µmol/L) was administered after a stable precontraction elicited by 1 µmol/L PE.

### *2.3. Data Analysis*

An MP100 system and AcqKnowledge 3.72 software from Biopac System Inc. (Goleta, CA, USA) were used to record and analyze changes in the vascular tone. All data are presented as mean ± SE, and *n* indicates the number of vascular segments tested in myography experiments or the number of animals tested in the case of body weight, blood glucose and serum phosphorylcholine levels. Maximal changes of the vascular tone were calculated as a percentage of precontraction. In order to evaluate the temporal pattern of nSMase-induced vasoactive responses, individual curves were constructed and averaged

showing the changes of vascular tone for 20 minutes after the application of nSMase. Area under curve (AUC) values were calculated from the individual experiments for quantification of the overall vasoactive effect. The statistical analysis was performed using the GraphPad Prism software v.6.07 from GraphPad Software Inc. (La Jolla, CA, USA). Student's unpaired *t* test was applied when comparing two variables, a *p* value of less than 0.05 was considered to be statistically significant. Effects of cumulative doses of PE and ACh were evaluated by dose-response curve fitting for determination of $E_{max}$ and $EC_{50}$ values.

### *2.4. Reagents*

All reagents in this study including nSMase were purchased from Sigma-Aldrich (St. Louis, MO, USA), except SQ-29548 which was from Santa Cruz Biotechnology (Dallas, TX, USA).

## 3. Results

First, we verified the general metabolic and vascular phenotype of T2DM mice tested in the present study. Db/db mice reportedly develop obesity with elevated blood glucose levels and insulin resistance [42-44]. Accordingly, the body weight showed almost two-fold (Fig. 1A), whereas blood glucose levels three-fold increase (Fig. 1B) in db/db mice as compared to non-diabetic control littermates. Furthermore, the serum phosphorylcholine level was also significantly increased in the diabetic group (Fig. 1C), which is consistent with the reported enhancement of SMase activity in type 2 diabetes [13-15]. Vessels of db/db animals showed marked endothelial dysfunction indicated by the impairment of the dose-response relationship of ACh-induced vasorelaxation after precontraction with 10 µmol/L PE (Fig. 1D). The $E_{max}$ value decreased to 50.8±2.0% in diabetic vessels as compared controls (65.8±3.9%). However, there was no significant difference in the $EC_{50}$ values (34.7±16.0 nM vs. 55.7±15.7 nM) indicating unchanged potency in spite of reduced efficacy of endogenous NO upon stimulation of eNOS by ACh. In contrast, reactivity of the vascular smooth muscle to NO remained unaltered, as neither the $E_{max}$ (105.2±1.8% vs. 103.3±2.2%) nor the $EC_{50}$ (10.7±1.3 nM vs. 14.1±2.0 nM) values of sodium nitroprusside-induced vasorelaxation differed in vessels of db/db animals as compared to controls (Fig.

1E). Taken together, these results confirm the T2DM-like metabolic and vascular phenotypes in db/db mice and suggest the in vivo enhancement of SMase activity as well.

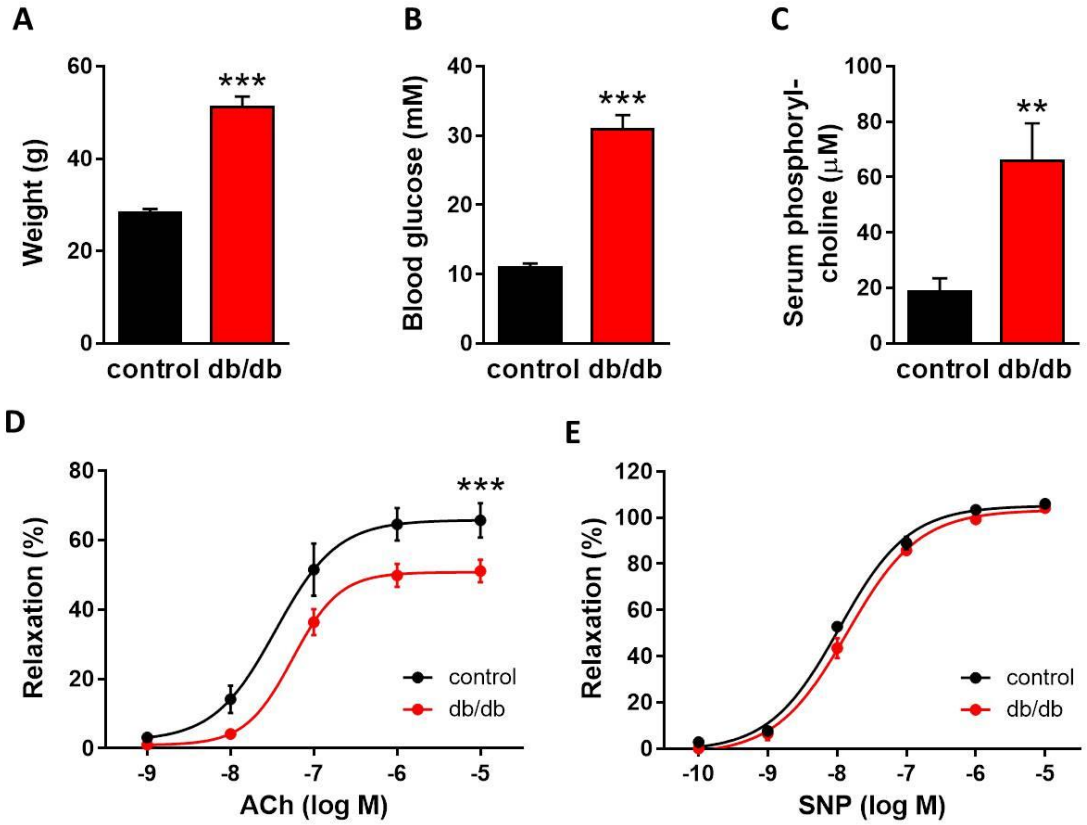


**Figure 1. Manifestation of the metabolic and vascular phenotype of T2DM in db/db mice.** Body weight (A), as well as non-fasting blood glucose (B) and serum phosphorylcholine levels (C) are increased in db/db mice as compared to controls (**p<0.01, ***p<0.001 vs. control group, Student's unpaired *t* test, n=13-22). ACh-induced relaxation diminished (D), while the reactivity of the vascular smooth muscle to sodium nitroprusside (SNP) remained unaltered (E) in vessels of db/db mice as compared to controls (mean ± SEM, ****p*<0.001 vs control, dose-response curve fitted to n=12-24)

Next, we determined the effect of nSMase on the active tone of control and db/db vessels (Fig. 2A). After 10 µmol/L PE-induced precontraction, 0.2 U/ml nSMase elicited additional contraction in control vessels that reached its maximum at 7.2 min before relaxing back to the pre-SMase level by the end of the 20-min observation period. In contrast, nSMase in db/db vessels elicited completely different responses. After a marked initial relaxation elicited by 0.2 U/ml nSMase during the first 5 minutes, the tone of the db/db vessels remained in a relaxed state below the level of the initial tension. From the shape of the

tension curve it appeared that in addition to the overriding relaxation there was a delayed and transient constriction response, with a time course similar to that observed in control vessels, but it was unable to overcome the robust dilatation. Evaluation of the AUC (Fig. 2B) and the maximal changes in the vascular tone (Fig. 2C) also supported the conclusion that there is a marked difference in the vascular effects of nSMase between control and db/db mice: whereas in the former contraction dominates, the latter is characterized by reduction of the vascular tone.

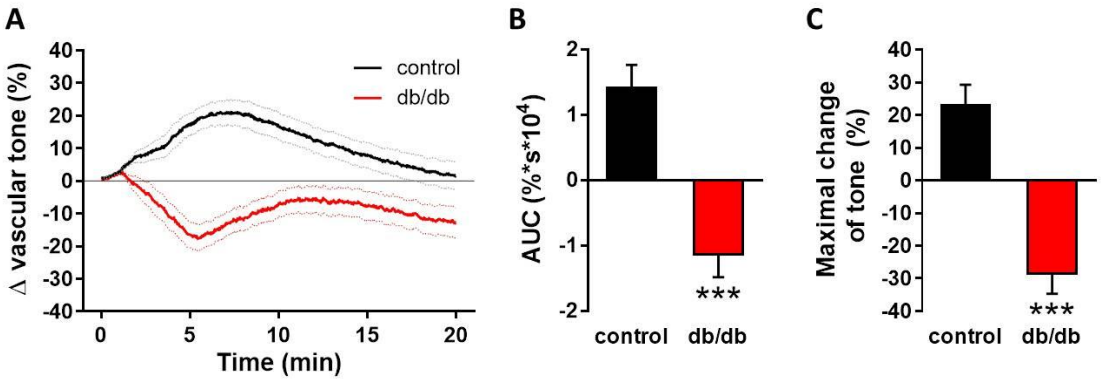


**Figure 2. Effects of nSMase on the vascular tone.** Application of 0.2 U/ml nSMase evoked a complex vascular effect with dominant contraction in control vessels and a more pronounced relaxation in vessels of db/db mice. Black and red lines on panel A represent average changes in tension of 10 µmol/L PE precontracted vessels of control and db/db mice, respectively (dotted lines represent SEM). Both area under curve values (B) and maximal tension changes (C) were significantly different in vessels from db/db animals as compared to controls (mean±SEM, Student's unpaired *t* test, ***$p$<0.001 vs control, n=41-43).

Our next aim was to dissect the constrictor and relaxant components of the vascular tension changes in response to nSMase. In porcine coronary arteries [26] as well as in carotid arteries of spontaneously hypertensive rats [35-37] prostanoids acting on thromboxane prostanoid receptors (TP) have been implicated in mediating the vasoconstrictor effect of SMase. Therefore, we hypothesized that TP receptors also mediate the nSMase-induced vasoconstriction in our murine aorta model. In order to test this hypothesis, the TP receptor antagonist SQ 29,548 was administered to the organ chambers 30 min prior to administration of nSMase. Blockade of TP receptors not only

abolished the vasoconstriction, but also converted it to a transient vasorelaxation in control vessels (Fig. 3A). The maximum of the relaxation was reached at 5.5 minutes after the administration of nSMase, and the vascular tone returned to the baseline after 10 minutes. TP receptor inhibition markedly changed the vascular response to nSMase also in the db/db group: the vasorelaxation was enhanced to more than 70% and reached its maximum at 6.5 minutes. After its peak, the relaxation decreased but the vascular tone failed to return to the pre-SMase level even after 20 minutes. Both the AUC (Fig. 3B) and the peak vasorelaxation (Fig. 3C) values showed marked differences between the two experimental groups, indicating that the strongly enhanced and prolonged vasorelaxant capacity is responsible for the differences between the vasoactive effects of nSMase in db/db and control vessels. This finding was very surprising in the light of the diminished ACh-induced vasorelaxation we observed in db/db animals (Fig. 1D), and was not consistent with the large body of literary data indicating diminished endothelium-dependent vasorelaxation in T2DM.

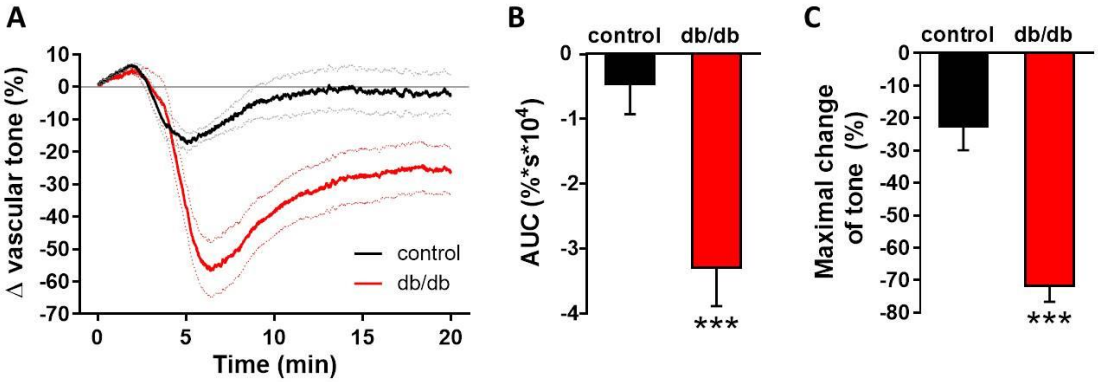


**Figure 3. Effects of TP receptor blockade on nSMase-induced changes of the vascular tone.** After inhibition of the TP receptor by 1 µM SQ 29,548, 0.2 U/ml nSMase relaxed both db/db and control vessels, with a significantly higher relaxation in the db/db group (A). Black and red lines on panel A represent average tension changes of precontracted vessels of control and db/db mice, respectively, whereas dotted lines represent SEM. Both area under curve values (B) and maximal tension changes (C) were significantly different in vessels from db/db animals as compared to controls (mean±SEM, Student's unpaired *t* test, ***$p$<0.001 vs control, n=15).

Finally, we aimed to analyze the mechanism of the enhanced nSMase-induced vasorelaxation in vessels of db/db mice. Theoretically, it could be due to the enhancement of eNOS-mediated vasorelaxation or to the onset of an NO-independent mechanism. To clarify this question, the vessels were incubated with the NOS inhibitor L-NAME (100 µM) in addition to the TP receptor blocker SQ 29,548 (1 µM) for 30 min prior to 0.2 U/ml nSMase administration. L-NAME at a concentration of 100 µM completely abolished the vasorelaxation observed in the presence of 1 µM SQ 29,548 both in control and in db/db vessels (Fig. 4A). There were no significant differences between the two groups either in the AUC (Fig. 4B), or in the maximal change of tension values (Fig. 4C). These results indicate that the same secondary signaling pathways – namely TP receptors and eNOS – mediate the vasoactive effects of nSMase in health and T2DM.

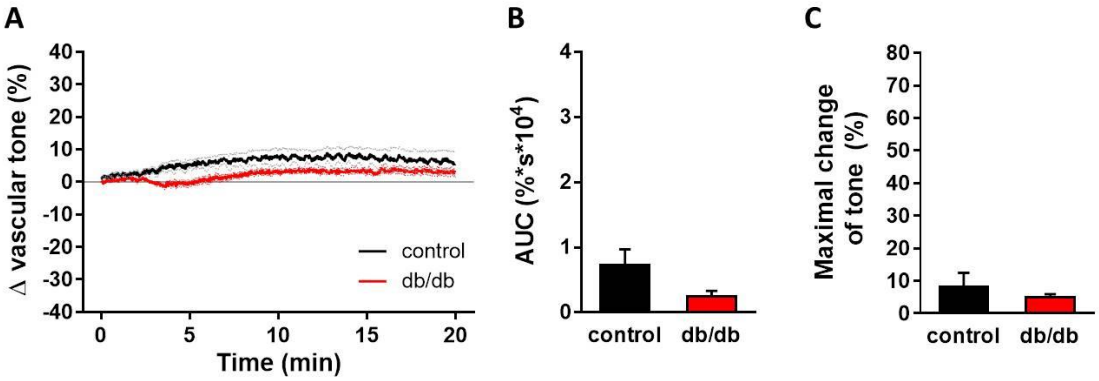


**Figure 4. Effects of combined TP receptor and NOS blockade on nSMase-induced changes of the vascular tone.** After incubation of the vessels with 1 µM SQ 29,548 and 100 µM L-NAME for 30 minutes, 0.2 U/ml nSMase could no longer evoke a tension change in the thoracic aorta of control or db/db mice (A). Black and red lines on panel A represent average tension changes of PE (10 µmol/L) precontracted vessels of control and db/db mice, respectively (dotted lines represent SEM). Area under curve values (B) and maximal tension changes (C) were not different in vessels from db/db animals as compared to controls (mean±SEM, n = 4-4).

## 4. Discussion

Findings of the present study indicate that nSMase-induced changes of vascular tension involve both vasoconstriction and vasorelaxation in murine vessels. Our results suggest that the former is mediated by release of prostanoids and activation of TP receptors, whereas the latter is mediated by eNOS. Surprisingly, nSMase-induced eNOS-mediated vasorelaxation is markedly enhanced in vessels of db/db mice in spite of the endothelial dysfunction indicated by the diminished vasorelaxation by ACh. Therefore, nSMase appears to be able to induce enhanced NO release from endothelial cells in T2DM.

Vasoconstriction in response to SMase has been reported in a number of studies, although the mechanisms mediating this effect appear to be highly variable depending on the experimental conditions including species, vascular region, and integrity of the endothelium (see Table 1). Release of prostanoids and consequent activation of TP receptors have been proposed in porcine coronary arteries [26] as well as in carotid arteries of spontaneously hypertensive rats [35-37]. In our study nSMase-induced contraction was found to be TP-receptor-dependent in both control and db/db mice, indicating that nSMase stimulates the release of $TXA_2$ from the aortic rings.

There might be at least three different sources for SMase-induced arachidonic acid formation that is necessary for $TXA_2$ production [45]. One such possibility is that diacyl glycerol (DAG) would accumulate while sphingomyelin synthase converts the newly generated ceramide back to sphingomyelin, and DAG lipases would provide arachidonic acid for the production of $TXA_2$ [46]. Another mechanism might relate to the observation that ceramide-1-phosphate can allosterically activate phospholipase $A_2$ ($PLA_2$) [47], which leads to arachidonic acid formation [48]. It might be important in this context that the gene encoding ceramide kinase (CERK) is upregulated in T2DM [49]. Finally, S1P has been reported recently to regulate prostanoid production in a S1P receptor-dependent manner [50].

Vasorelaxation in response to nSMase appears to be endothelial NO-dependent, as L-NAME completely abolished the decrease of vascular tone in both control and db/db vessels. Without L-NAME the relaxation was dramatically increased in db/db-derived vascular rings. This is unexpected, because endothelial dysfunction with consequential

decrease on the vasorelaxant capacity is considered to be a hallmark for T2DM-like conditions. A potential explanation may be related to the altered structure of the plasma membrane in T2DM [51]. Normally, SM represents about 10-20% of the lipids in the plasma membrane, mostly residing in the outer leaflet. However, most of these are found in the caveolae, and SMase is thought to be a regulator of lipid microdomains [52, 53]. Pilarczyk and colleagues provided evidence that in db/db mice the endothelial lining of the aorta contains ten-fold larger lipid raft areas enriched in SM as compared to controls [51]. This arrangement might be related to the decreased NO-release in T2DM, as eNOS is inhibited by caveolin-1 [54], which is considered to be an important regulator of eNOS [55-57]. In our experimental setting, nSMase-induced degradation of sphingomyelin could interfere with this caveolar structure and induce the detachment of eNOS from caveolin-1, leading to high amounts of NO released from the endothelium of db/db vascular rings. This hypothesis is supported by the observation of Mogami et al. [33] indicating that SMase causes endothelium-dependent vasorelaxation through $Ca^{2+}$-independent endothelial NO production in bovine aortic valves and coronary arteries. They also reported SMase-induced translocation of endothelial NOS from plasma membrane caveolae to the intracellular region. Furthermore, protein expression levels of caveolin-1 were reported to be significantly higher in the aorta of db/db mice, and this was thought to be related to the impaired aortic relaxation of C57BL/KsJ mice [58]. Still, we cannot rule out the possibility that the enhanced sphingolipid content of the membrane augments the release of sphingolipid mediators such as ceramide, and consequently enhances the ceramide-related vasorelaxation reported in non-diabetic models [27-29, 32]. It has to be emphasized, though, that the ceramide-related pathway might be involved in the SMase-induced contractions as well [30, 35]. Finally, the potentially increased NO-sensitivity of guanylate cyclase (sGC) [59], which could be related to the dysfunctional NO-release observed in T2DM, should also be considered, as this would sensitize sGC to NO resulting in enhanced NO-mediated vasorelaxation. However, this mechanism can be excluded in our present experiments, since the SNP dose-response curve remained unchanged in db/db vessels (Fig. 1E), indicating that the sensitivity of the vascular smooth muscle to NO was not upregulated.

Sphingolipid metabolism is markedly altered in T2DM and related conditions [60-64], and the observed changes in endothelial lipid rafts [51] might be a consequence of the

disrupted plasma membrane lipid metabolism. On the other hand, T2DM has several characteristics that resemble a chronic inflammatory disease [65]. Cytokines that accumulate in chronic inflammation, such as tumor necrosis factor alpha (TNF-α) and interleukin 1 beta (IL-1β) can also induce marked changes in sphingolipid metabolism [6, 66, 67]. Our observation that the serum phosphorylcholine levels were increased in the db/db group is strong indicator of the altered in vivo sphingolipid metabolism in our animal model and agrees with the literature.

As a limitation of our study it has to be mentioned that the characteristics of the pathophysiological conditions in the db/db mouse model differ from those of human T2DM in some aspects [68]. For example, db/db mice do not necessarily develop hypertension and may have high levels of HDL and reduced tendency to atherosclerosis [69]. Therefore, due to the more severe endothelial dysfunction, the enhancement of nSMase-induced eNOS-mediated vasorelaxation may be limited in humans with T2DM. A further limitation of our study is that we tested only one single dose of nSMase. This 0.2 U/ml dose represents the upper range used in the literature [26-30, 32-35], as our aim was to evaluate the consequences of a robust activation of sphingomyelinase degradation. Further studies may aim to elucidate the exact dose-response relationship for SMase-induced vasorelaxation and vasoconstriction in db/db or other T2DM-related conditions, which may also help to clarify the exact molecular mechanisms involved.

## 5. Conclusions

Administration of nSMase induces TP-receptor-mediated vasoconstriction and eNOS-mediated vasorelaxation in murine vessels. In spite of endothelial dysfunction in db/db mice the vasorelaxant effect of nSMase is markedly augmented. SMase-mediated disruption of SM in endothelial lipid rafts might represent a possible mechanism responsible for enhanced NO generation in T2DM. An intriguing interpretation of our finding is that retraction of eNOS in sphingomyelin-rich microdomains of the endothelial plasma membrane could contribute significantly to the development of vascular dysfunction in T2DM.

## Conflict of interest

The authors declare no conflict of interest.

## Acknowledgements

This study has been supported by the European Foundation for the Study of Diabetes (EFSD/Servier Grant), the Hungarian National Research, Development and Innovation Office (OTKA PD-83803, OTKA K-112964, OTKA K-115607 and NVKP_16-1-2016-0042) and by the Hungarian Academy of Sciences (BO/00470/14 Bolyai Fellowship). The authors are grateful to Margit Kerék for expert technical assistance and to Dr. Erzsébet Fejes for critically reading the manuscript.

## Author contributions

ZB, GT and ÉR designed research; ÉR, LK, ZS, DK, AP performed experiments; ÉR, LK, ZS, DK, AP analyzed data and prepared figures; ÉR, LK, KL, GT and ZB wrote the paper.

## References

1. Peters, S.L. and A.E. Alewijnse, *Sphingosine-1-phosphate signaling in the cardiovascular system.* Curr Opin Pharmacol, 2007. **7**(2): p. 186-92.
2. Igarashi, J. and T. Michel, *Sphingosine-1-phosphate and modulation of vascular tone.* Cardiovasc Res, 2009. **82**(2): p. 212-20.
3. Kerage, D., D.N. Brindley, and D.G. Hemmings, *Review: novel insights into the regulation of vascular tone by sphingosine 1-phosphate.* Placenta, 2014. **35 Suppl**: p. S86-92.
4. Proia, R.L. and T. Hla, *Emerging biology of sphingosine-1-phosphate: its role in pathogenesis and therapy.* J Clin Invest, 2015. **125**(4): p. 1379-87.
5. Hemmings, D.G., *Signal transduction underlying the vascular effects of sphingosine 1-phosphate and sphingosylphosphorylcholine.* Naunyn Schmiedebergs Arch Pharmacol, 2006. **373**(1): p. 18-29.
6. De Palma, C., et al., *Endothelial nitric oxide synthase activation by tumor necrosis factor alpha through neutral sphingomyelinase 2, sphingosine kinase 1, and sphingosine 1 phosphate receptors: a novel pathway relevant to the pathophysiology of endothelium.* Arterioscler Thromb Vasc Biol, 2006. **26**(1): p. 99-105.
7. Fyrst, H. and J.D. Saba, *An update on sphingosine-1-phosphate and other sphingolipid mediators.* Nat Chem Biol, 2010. **6**(7): p. 489-97.
8. Meyer zu Heringdorf, D. and K.H. Jakobs, *Lysophospholipid receptors: signalling, pharmacology and regulation by lysophospholipid metabolism.* Biochim Biophys Acta, 2007. **1768**(4): p. 923-40.
9. Strub, G.M., et al., *Extracellular and intracellular actions of sphingosine-1-phosphate.* Adv Exp Med Biol, 2010. **688**: p. 141-55.
10. Hla, T. and A.J. Dannenberg, *Sphingolipid signaling in metabolic disorders.* Cell Metab, 2012. **16**(4): p. 420-34.
11. Ernst, A.M. and B. Brugger, *Sphingolipids as modulators of membrane proteins.* Biochim Biophys Acta, 2014. **1841**(5): p. 665-70.

12. Adada, M., C. Luberto, and D. Canals, *Inhibitors of the sphingomyelin cycle: Sphingomyelin synthases and sphingomyelinases.* Chem Phys Lipids, 2016. **197**: p. 45-59.
13. Pavoine, C. and F. Pecker, *Sphingomyelinases: their regulation and roles in cardiovascular pathophysiology.* Cardiovasc Res, 2009. **82**(2): p. 175-83.
14. Shamseddine, A.A., M.V. Airola, and Y.A. Hannun, *Roles and regulation of neutral sphingomyelinase-2 in cellular and pathological processes.* Adv Biol Regul, 2015. **57**: p. 24-41.
15. Russo, S.B., J.S. Ross, and L.A. Cowart, *Sphingolipids in obesity, type 2 diabetes, and metabolic disease.* Handb Exp Pharmacol, 2013(216): p. 373-401.
16. Cowart, L., *Sphingolipids: players in the pathology of metabolic disease.* Trends Endocrinol Metab, 2009. **20**(1): p. 34-42.
17. Hannun, Y. and L. Obeid, *The Ceramide-centric universe of lipid-mediated cell regulation: stress encounters of the lipid kind.* J Biol Chem, 2002. **277**(29): p. 25847-50.
18. Sawai, H. and Y. Hannun, *Ceramide and sphingomyelinases in the regulation of stress responses.* Chem Phys Lipids, 1999. **102**(1-2): p. 141-7.
19. Hannun, Y. and C. Luberto, *Ceramide in the eukaryotic stress response.* Trends Cell Biol, 2000. **10**(2): p. 73-80.
20. van Meer, G. and J. Holthuis, *Sphingolipid transport in eukaryotic cells.* Biochim Biophys Acta, 2000. **1486**(1): p. 145-70.
21. Holland, W. and S. Summers, *Sphingolipids, insulin resistance, and metabolic disease: new insights from in vivo manipulation of sphingolipid metabolism.* Endocr Rev, 2008. **29**(4): p. 381-402.
22. Unger, R. and L. Orci, *Lipoapoptosis: its mechanism and its diseases.* Biochim Biophys Acta, 2002. **1585**(2-3): p. 202-12.
23. Boden, G., *Pathogenesis of type 2 diabetes. Insulin resistance.* Endocrinol Metab Clin North Am, 2001. **30**(4): p. 801-15, v.
24. Samad, F., *Contribution of sphingolipids to the pathogenesis of obesity.* FUTURE LIPIDOLOGY, 2007: p. 625-639.
25. Symons, J.D. and E.D. Abel, *Lipotoxicity contributes to endothelial dysfunction: a focus on the contribution from ceramide.* Rev Endocr Metab Disord, 2013. **14**(1): p. 59-68.
26. Murohara, T., et al., *Effects of sphingomyelinase and sphingosine on arterial vasomotor regulation.* J Lipid Res, 1996. **37**(7): p. 1601-8.
27. Johns, D.G., et al., *Ceramide-induced vasorelaxation: An inhibitory action on protein kinase C.* Gen Pharmacol, 1999. **33**(5): p. 415-21.
28. Johns, D.G., H. Osborn, and R.C. Webb, *Ceramide: a novel cell signaling mechanism for vasodilation.* Biochem Biophys Res Commun, 1997. **237**(1): p. 95-7.
29. Zheng, T., et al., *Effects of neutral sphingomyelinase on phenylephrine-induced vasoconstriction and Ca(2+) mobilization in rat aortic smooth muscle.* Eur J Pharmacol, 2000. **391**(1-2): p. 127-35.
30. Zheng, T., et al., *Sphingomyelinase and ceramide analogs induce contraction and rises in [Ca(2+)](i) in canine cerebral vascular muscle.* Am J Physiol Heart Circ Physiol, 2000. **278**(5): p. H1421-8.
31. Altura, B.M., et al., *Sphingomyelinase and ceramide analogs induce vasoconstriction and leukocyte-endothelial interactions in cerebral venules in the intact rat brain: Insight into mechanisms and possible relation to brain injury and stroke.* Brain Res Bull, 2002. **58**(3): p. 271-8.
32. Jang, G.J., et al., *C2-ceramide induces vasodilation in phenylephrine-induced pre-contracted rat thoracic aorta: role of RhoA/Rho-kinase and intracellular Ca2+ concentration.* Naunyn Schmiedebergs Arch Pharmacol, 2005. **372**(3): p. 242-50.
33. Mogami, K., H. Kishi, and S. Kobayashi, *Sphingomyelinase causes endothelium-dependent vasorelaxation through endothelial nitric oxide production without cytosolic Ca(2+) elevation.* FEBS Lett, 2005. **579**(2): p. 393-7.

34. Cogolludo, A., et al., *Activation of neutral sphingomyelinase is involved in acute hypoxic pulmonary vasoconstriction.* Cardiovasc Res, 2009. **82**(2): p. 296-302.
35. Spijkers, L.J., et al., *Hypertension is associated with marked alterations in sphingolipid biology: a potential role for ceramide.* PLoS One, 2011. **6**(7): p. e21817.
36. Spijkers, L.J., et al., *Antihypertensive treatment differentially affects vascular sphingolipid biology in spontaneously hypertensive rats.* PLoS One, 2011. **6**(12): p. e29222.
37. van den Elsen, L.W., et al., *Dietary fish oil improves endothelial function and lowers blood pressure via suppression of sphingolipid-mediated contractions in spontaneously hypertensive rats.* J Hypertens, 2014. **32**(5): p. 1050-8; discussion 1058.
38. Horvath, B., P. Orsy, and Z. Benyo, *Endothelial NOS-mediated relaxations of isolated thoracic aorta of the C57BL/6J mouse: a methodological study.* J Cardiovasc Pharmacol, 2005. **45**(3): p. 225-31.
39. Hojjati, M.R. and X.C. Jiang, *Rapid, specific, and sensitive measurements of plasma sphingomyelin and phosphatidylcholine.* J Lipid Res, 2006. **47**(3): p. 673-6.
40. Raines, M.A., R.N. Kolesnick, and D.W. Golde, *Sphingomyelinase and ceramide activate mitogen-activated protein kinase in myeloid HL-60 cells.* J Biol Chem, 1993. **268**(20): p. 14572-5.
41. Linardic, C.M. and Y.A. Hannun, *Identification of a distinct pool of sphingomyelin involved in the sphingomyelin cycle.* J Biol Chem, 1994. **269**(38): p. 23530-7.
42. Aasum, E., et al., *Age-dependent changes in metabolism, contractile function, and ischemic sensitivity in hearts from db/db mice.* Diabetes, 2003. **52**(2): p. 434-41.
43. Coleman, D.L., *Obese and diabetes: two mutant genes causing diabetes-obesity syndromes in mice.* Diabetologia, 1978. **14**(3): p. 141-8.
44. Do, O.H., et al., *The secretory deficit in islets from db/db mice is mainly due to a loss of responding beta cells.* Diabetologia, 2014. **57**(7): p. 1400-9.
45. Ramadan, F.M., et al., *Endothelial cell thromboxane production and its inhibition by a calcium-channel blocker.* Ann Thorac Surg, 1990. **49**(6): p. 916-9.
46. Epand, R.M., et al., *Diacylglycerol Kinase-epsilon: Properties and Biological Roles.* Front Cell Dev Biol, 2016. **4**: p. 112.
47. Subramanian, P., et al., *Anionic lipids activate group IVA cytosolic phospholipase A2 via distinct and separate mechanisms.* J Lipid Res, 2007. **48**(12): p. 2701-8.
48. Pettus, B.J., et al., *Ceramide kinase mediates cytokine- and calcium ionophore-induced arachidonic acid release.* J Biol Chem, 2003. **278**(40): p. 38206-13.
49. Mitsutake, S., et al., *Ceramide kinase deficiency improves diet-induced obesity and insulin resistance.* FEBS Lett, 2012. **586**(9): p. 1300-5.
50. Machida, T., et al., *Cellular function and signaling pathways of vascular smooth muscle cells modulated by sphingosine 1-phosphate.* J Pharmacol Sci, 2016. **132**(4): p. 211-217.
51. Pilarczyk, M., et al., *Endothelium in spots--high-content imaging of lipid rafts clusters in db/db mice.* PLoS One, 2014. **9**(8): p. e106065.
52. Mitsutake, S., et al., *Dynamic modification of sphingomyelin in lipid microdomains controls development of obesity, fatty liver, and type 2 diabetes.* J Biol Chem, 2011. **286**(32): p. 28544-55.
53. Romiti, E., et al., *Localization of neutral ceramidase in caveolin-enriched light membranes of murine endothelial cells.* FEBS Lett, 2001. **506**(2): p. 163-8.
54. Jasmin, J.F., Frank, P.G., Lisanti, M.P., *Caveolins and Caveolae: Roles in Signaling and Disease Mechanism.* Advances in Experimental Medicine and Biology, New York: Springer Science+Business Media, LCC., 2012: p. 3–13.
55. Garcia-Cardena, G., et al., *Dissecting the interaction between nitric oxide synthase (NOS) and caveolin. Functional significance of the nos caveolin binding domain in vivo.* J Biol Chem, 1997. **272**(41): p. 25437-40.
56. Frank, P.G., et al., *Caveolin, caveolae, and endothelial cell function.* Arterioscler Thromb Vasc Biol, 2003. **23**(7): p. 1161-8.

57. Shaul, P.W., *Regulation of endothelial nitric oxide synthase: location, location, location.* Annu Rev Physiol, 2002. **64**: p. 749-74.
58. Lam, T.Y., et al., *Impairment of the vascular relaxation and differential expression of caveolin-1 of the aorta of diabetic +db/+db mice.* Eur J Pharmacol, 2006. **546**(1-3): p. 134-41.
59. Miller, M.A., et al., *Adenylate and guanylate cyclase activity in the penis and aorta of the diabetic rat: an in vitro study.* Br J Urol, 1994. **74**(1): p. 106-11.
60. Samad, F., et al., *Altered adipose and plasma sphingolipid metabolism in obesity: a potential mechanism for cardiovascular and metabolic risk.* Diabetes, 2006. **55**(9): p. 2579-87.
61. Arora, T., et al., *Roux-en-Y Gastric Bypass Surgery Induces Early Plasma Metabolomic and Lipidomic Alterations in Humans Associated with Diabetes Remission.* PLoS One, 2015. **10**(5): p. e0126401.
62. Fox, T.E., et al., *Circulating sphingolipid biomarkers in models of type 1 diabetes.* J Lipid Res, 2011. **52**(3): p. 509-17.
63. Gorska, M., E. Baranczuk, and A. Dobrzyn, *Secretory Zn2+-dependent sphingomyelinase activity in the serum of patients with type 2 diabetes is elevated.* Horm Metab Res, 2003. **35**(8): p. 506-7.
64. Gorska, M., A. Dobrzyn, and M. Baranowski, *Concentrations of sphingosine and sphinganine in plasma of patients with type 2 diabetes.* Med Sci Monit, 2005. **11**(1): p. CR35-8.
65. Donath, M.Y. and S.E. Shoelson, *Type 2 diabetes as an inflammatory disease.* Nat Rev Immunol, 2011. **11**(2): p. 98-107.
66. Dressler, K.A., S. Mathias, and R.N. Kolesnick, *Tumor necrosis factor-alpha activates the sphingomyelin signal transduction pathway in a cell-free system.* Science, 1992. **255**(5052): p. 1715-8.
67. Wiegmann, K., et al., *Functional dichotomy of neutral and acidic sphingomyelinases in tumor necrosis factor signaling.* Cell, 1994. **78**(6): p. 1005-15.
68. Wang, B., P.C. Chandrasekera, and J.J. Pippin, *Leptin- and leptin receptor-deficient rodent models: relevance for human type 2 diabetes.* Curr Diabetes Rev, 2014. **10**(2): p. 131-45.
69. Cohen, M.P., et al., *Evolution of renal function abnormalities in the db/db mouse that parallels the development of human diabetic nephropathy.* Exp Nephrol, 1996. **4**(3): p. 166-71.